

#### **OPEN ACCESS**

EDITED BY Galina Sud'ina, Lomonosov Moscow State University, Russia

REVIEWED BY

Palsamy Periyasamy, University of Nebraska Medical Center, United States Pranay Wal, Pranveer Singh Institute of Technology PSIT, India

\*CORRESPONDENCE
Palash Mandal,

□ palashmandal.bio@charusat.ac.in

RECEIVED 07 August 2025 REVISED 18 October 2025 ACCEPTED 21 October 2025 PUBLISHED 10 November 2025

#### CITATION

Chadha P, Aghara H, Solanki H, Patel M, Sharma D, Thiruvenkatam V and Mandal P (2025) Modulation of  $TNF\alpha$ -driven neuroinflammation by Gardenin A: insights from in vitro, in vivo, and in silico studies. Front. Pharmacol. 16:1681403. doi: 10.3389/fphar.2025.1681403

#### COPYRIGHT

© 2025 Chadha, Aghara, Solanki, Patel, Sharma, Thiruvenkatam and Mandal. This is an openaccess article distributed under the terms of the Creative Commons Attribution License (CC BY).

The use, distribution or reproduction in other forums is permitted, provided the original author(s) and the copyright owner(s) are credited and that the original publication in this journal is cited, in accordance with accepted academic practice. No use, distribution or reproduction is permitted which does not comply with these terms.

# Modulation of TNF $\alpha$ -driven neuroinflammation by Gardenin A: insights from *in vitro*, *in vivo*, and *in silico* studies

Prashsti Chadha<sup>1</sup>, Hiral Aghara<sup>1</sup>, Harshrajsinh Solanki<sup>1</sup>, Manali Patel<sup>1</sup>, Dhrubjyoti Sharma<sup>2</sup>, Vijay Thiruvenkatam<sup>2</sup> and Palash Mandal<sup>1\*</sup>

<sup>1</sup>Department of Biological Sciences, PD Patel Institute of Applied Sciences (PDPIAS), Charotar University of Science and Technology, Changa, Gujarat, India, <sup>2</sup>Department of Biological Sciences and Engineering, Indian Institute of Technology Gandhinagar, Palaj, Gujarat, India

**Introduction:** Chronic alcohol consumption is a major contributor to neuroinflammation, oxidative stress, and blood-brain barrier (BBB) disruption, leading to significant neuronal injury. Traditional therapies for alcohol use disorder (AUD) predominantly target behavioral and receptor-based mechanisms, often neglecting the direct pathophysiological impacts of alcohol on brain tissue. This study explores the neuroprotective potential of Gardenin A (GarA), a hexa-methoxylated flavone, in counteracting alcohol-induced inflammation and physiological damage.

Methods: In vitro experiments utilized SH-SY5Y neuroblastoma cells treated with varying concentrations of GarA, assessing cell viability, nuclear integrity, oxidative stress, and gene expression. In vivo experiments involved the administration of ethanol alongside GarA at doses of 50 and 100 mg/kg body weight to male Wistar rats. Subsequent brain tissue analysis employed histological and immunohistochemical methods to evaluate structural preservation and cellular responses. Key molecular targets were examined, including vimentin, brainderived neurotrophic factor (BDNF), and Claudin5. Protein levels of inflammatory markers and antioxidant enzymes were quantified using ELISA, providing detailed insights into the biochemical pathways involved. Complementary in silico methods, such as molecular docking and network pharmacology, were employed to elucidate the mechanistic interactions and predict potential molecular binding sites.

**Results:** The treatment with GarA resulted in enhanced neuronal viability and a reduction in ethanol-induced oxidative stress *in vitro. In vivo* results demonstrated preservation of brain architecture, attenuation of astroglial reactivity, and significant downregulation of tumor necrosis factor-alpha (TNF $\alpha$ ), a key mediator of neuroinflammation. Additionally, GarA was associated with restored BDNF expression and upregulated antioxidant markers like HO-1 and Nrf2, maintaining neurovascular integrity and neurotrophic balance.

**Discussion:** GarA demonstrates neuroprotective potential, with evidence suggesting modulation of neuroinflammation and oxidative stress that may involve  $\mathsf{TNF}\alpha$  and BDNF pathways. These promising findings suggest potential therapeutic applications for GarA in addressing alcohol-related neurodegeneration. Future research focusing on clinical trials may prove

helpful in validating these preclinical findings. Expanding studies to include diverse animal models and exploring combinatory treatments with existing AUD therapies could enhance understanding and application. Such efforts may pave the way for incorporating GarA into comprehensive pharmacotherapeutic strategies aimed at mitigating the neuropathological effects of chronic alcohol consumption.

KEVWODDS

alcohol-induced neuroinflammation, herbal therapeutics, gardenin A, blood-brainbarrier,  $\mathsf{TNF}\alpha$ 

### 1 Introduction

Ethanol, a widely consumed psychoactive substance and Class I carcinogen, exerts neurotoxic effects through mechanisms involving oxidative stress, inflammation, and metabolic disruption (World Health Organization, 2024). Chronic exposure to ethanol is a well-established contributor to systemic toxicity and is a major risk factor for neurodegenerative disorders, including Alzheimer's (AD) and Parkinson's disease (PD). Globally, reports indicate that alcohol consumption has been steadily increasing over time.

While the liver is the primary site of ethanol metabolism, the brain is both susceptible and metabolically active, with the ability to oxidize ethanol via catalase and cytochrome P450 2E1 (CYP2E1), leading to nearly 80% of the neuronal alcohol metabolism (Beisswenger et al., 1985; Martínez et al., 2001; Galter et al., 2003; Zimatkin et al., 2006; Wilson and Matschinsky, 2020; Wen et al., 2022). Furthermore, astrocytes (a type of glial cell) have acetaldehyde dehydrogenase 2 (ALDH2) which leads to the formation of acetate, which contributes to severe intoxication and alcohol dependence (Carmichael et al., 1991; Volkow et al., 2013; Mews et al., 2019; Jin et al., 2021). Alcohol not only crosses the blood-brain barrier (BBB) but also disrupts its structural integrity, exacerbating neuroinflammatory responses (Vore and Deak, 2022). Hence ethanol's metabolism in neuronal tissue produces acetaldehyde and reactive oxygen species (ROS), leading to cellular redox imbalance, mitochondrial damage, and membrane destabilization. These mechanisms underlie its classification as a neurotoxic agent in toxicological studies.

The central nervous system (CNS) comprises four main types of glial cells: astrocytes, microglia, oligodendrocytes and their precursor cells, polydendrocytes. All of these are significantly impacted by alcohol exposure in terms of their growth, morphology, physiology, and gene expression (Miguel-Hidalgo, 2018). At low levels, alcohol can transiently activate microglia, eliciting neuroprotective responses. However, chronic exposure results in microglial overactivation and the release of proinflammatory cytokines. Among the critical mediators of alcoholinduced neurotoxicity, tumor necrosis factor-alpha (TNFα) plays a central pathogenic role, while proprotein convertase subtilisin/kexin type 9 (PCSK9) has been implicated as a novel neuroinflammatory mediator linking the liver-brain axis. Ethanol exposure upregulates TNFa and PCSK9 expression, which in turn amplifies the inflammatory milieu by stimulating microglial and astrocytic activation (accompanied by increased expression of intermediate filament protein such as vimentin) and downstream cytokines such as monocyte chemoattractant protein-1 (MCP-1), interleukin 1-beta (IL-1β), and interlukin-6 (IL-6) (Ward et al., 2009; Qin and Crews, 2012; Patel and Mandal, 2018; Anand et al., 2023).

Prolonged TNFα signaling contributes to neuronal apoptosis, BBB dysfunction, and synaptic loss - hallmarks of alcohol-induced cognitive decline. Ethanol-induced ROS and RNS production, coupled with ER stress, impairs tight junction proteins and compromises BBB integrity (Varadinova et al., 2019). Studies have shown that alcohol induced neuroinflammation, along with oxidative and endoplasmic reticulum (ER) stress, disrupts tight junctions (TJs) and compromises BBB integrity (Carrino et al., 2021; Wei et al., 2021). This further aggravates the inflammation by allowing the permeation of inflammatory cytokines and other immune cells from the peripheral nervous system (PNS) (Togre et al., 2024). In parallel, ethanol suppresses neurotrophic signaling, particularly the expression of BDNF, impairing neuronal survival, plasticity, and repair mechanisms (Tapia-Arancibia et al., 2001; Raivio et al., 2012; Martín-González et al., 2022).

Researchers worldwide are actively investigating the toxic effects of alcohol on the brain and are exploring potential therapeutic strategies to mitigate its impact. While most studies predominantly target alcohol dependence and withdrawal, fewer have addressed the underlying stress mechanisms in the brain caused by chronic alcohol overconsumption. A limited number of preclinical studies have evaluated natural compounds for their potential to alleviate alcohol-induced oxidative stress and inflammation, including resveratrol (Petrella et al., 2020), olive polyphenols (Carito et al., 2017), saffron and crocin (Bandegi et al., 2014) and minocycline (Motaghinejad et al., 2021). Additional research has focused on preventing or treating alcohol-induced neurodegenerative apoptosis using agents such as nicotinamide (Ieraci and Herrera, 2006) and epigallocatechin-3-gallate (EGCG) (Tiwari et al., 2010). Parallel studies have also explored the neuroprotective effect of these natural compounds in the context of neurodegenerative disorders. For instance, quercetin has been shown to mitigate mitochondrial dysfunction in PD (Kang et al., 2020), while baicalein exerts neuroprotection through its anti-inflammatory, antioxidant and anti-apoptotic properties (Lee et al., 2005; Li et al., 2012).

GarA, (C<sub>21</sub>H<sub>22</sub>O<sub>9</sub>) (molecular weight: 418.4 g/mol) a hexamethoxylated flavone, is found in various plant sources, including *Gardenia resinifera* Roth. (Toppo et al., 2017). and *Murraya paniculata* (Kinoshita and Firman, 1996). It has previously demonstrated hepatoprotective and antihyperlipidaemic properties against metabolism-associated liver disease (MASLD) in *in vitro* and *in vivo* models (Toppo et al., 2017) and against alcohol-induced liver and gut damage in an *in vitro* model (Chadha et al., 2025). GarA has also shown antioxidative and neuroprotective properties in a rat model of focal brain ischemia (Zhang et al., 2005), and has been found to facilitate neurite outgrowth in PC-12 cells, suggesting potential therapeutic

relevance for neurodegenerative conditions such as AD and PD (Chiu et al., 2013). It has anti-anxiety-like, anti-convulsant, and anti-depressant-like neuropharmacological activities in mice (Alonso-Castro et al., 2020) and anti-neuroinflammatory effects in the *Drosophila* model of PD (Maitra et al., 2021). Most importantly, recently (Hack et al., 2024) uncovered the potential of GarA to cross the BBB and protect against cognitive and motor dysfunction against PD.

Currently, three FDA-approved medications are available for the treatment of AUD, but these drugs primarily function by targeting neural receptors and are associated with notable limitations. For example, some of these drugs are contraindicated in individuals with comorbid conditions—naltrexone and disulfiram in those with advanced liver disease, acamprosate in cases of renal impairment, and disulfiram in patients with cognitive deficits (MacKillop et al., 2022; Agabio et al., 2024). Despite growing interest in flavonoid-based neuroprotection, little is known about their effect on ethanol-induced dysregulation of key molecular targets such as TNFa, PCSK9, MCP-1, Claudins, Vimentin, and BDNF. These markers are closely associated with oxidative stress response, tight junction integrity, and neuroinflammatory signaling. This study investigates the potential of GarA to influence TNFadriven neuroinflammatory cascades and associated molecular markers in ethanol-induced neurotoxicity, using an integrated in vitro, in vivo, and in silico approach.

### 2 Materials and methods

### 2.1 Materials

Culture media, supplements, antibiotic-antimycotic solution, fetal bovine serum (FBS), 1X phosphate buffered saline (PBS) and rat feed components were procured from HiMedia (Mumbai, India), unless specified otherwise. Retinoic acid (RA) for differentiation and Silymarin (SilM) for use as standard drug was obtained from Sigma-Aldrich (St. Louis, Missouri, United States). Antibodies for immunohistochemical staining were purchased from Thermo Scientific (anti-vimentin V9, MA5-11883) and Agilent Technologies (EnvisionTM HRP, Dako). Enzyme linked immunosorbent assay (ELISA) kits for rat TNFα (Cat. no. ELR-TNFa-1), rat BDNF (Cat. no. ELR-BDNF-1), rat IL-6 (Cat. no. ELR-IL6-1) and rat MCP-1 (Cat. no. ELR-MCP1-1) were purchased from RayBiotech Life, Inc. (Georgia, USA) and rat HO-1 (Cat. no. orb411280) and rat Nrf2 (Cat. no. orb781880) were purchased from Biorbyt LLC (North Carolina, USA).

### 2.2 Cell culture study

SH-SY5Y (RRID: CVCL\_0019), neuroblastoma cells were obtained from National Centre for Cell Science (NCCS, Pune, India) and were provided mycoplasma-free. Cells were cultured in Dulbecco's Modified Eagle Medium/ Nutrient Mixture F-12 Ham (DMEM/ F12, 1:1 ratio), supplemented with 10% FBS and 1% antibiotic and antimycotic solution, maintained at 37 °C and 5% CO<sub>2</sub> in a water-jacketed incubator. Cells were subcultured at 70%–80% confluency with adequate medium replenishment. For

experimental assays, cells were seeded at a density of  $1 \times 10^4$ cells per well in 96-well plates and  $5 \times 10^5$  cells per well in 6well plates. Cells between passage 25 - 30 were used for the experiments. For neuronal differentiation, cells were treated with 10 mM RA in low-serum medium (1%) for 3 days prior to treatment, following the protocol by (Bustos-Rangel et al., 2023) and validated using morphological changes using ImageJ neurite length analysis (Supplementary Figure S1; Supplementary Table S1). To minimize ethanol evaporation during treatments, plates were sealed with Parafilm (covering ~75% of the surface, allowing adequate gas exchange) and maintained in a water-jacketed incubator to ensure stable humidity and temperature. Ethanol-treated wells were placed toward the center of the plates, while untreated control wells were positioned at the periphery to minimize differential evaporation. In addition, medium containing ethanol was added to the unused spaces of the culture plates, which has been shown to further reduce evaporation (Rath et al., 2022).

### 2.3 Animal study

Animal experimentation was performed as per standard ethical ARRIVE (Animal research: reporting of *in vivo* Experiments) guidelines and approved (RPCP/IAEC/2023-24/R16) by the Institutional ethical committee of Charotar University of Science and Technology. Eight-to ten-week-old male Wistar rats (weighing 200–250 gm) were procured from SyncBio Research Pvt. Ltd. (Gujarat, India). Before beginning the study, the rats were caged in ambient conditions (25 °C  $\pm$  2 °C with relative humidity 55%  $\pm$  5%) with two rats per cage. They were provided with a standard chow diet and water *ad libitum*, and allowed to acclimatize for a period of 7 days. They were accommodated in 12 h dark and light cycles throughout the study.

# 2.4 Preparation of GarA stocks for *in vitro* and *in vivo* experiments

Pure GarA was previously extracted, isolated from *G. resinifera* Roth. gum and characterized in the lab (Chadha et al., 2025) was utilized for this study. For the *in vitro* study, the stock solutions (1 mg/mL and 100 μg/mL) were prepared using dimethyl sulfoxide (DMSO) and 1X PBS, ensuring the final DMSO concentration did not exceed 0.1%. For *in vivo* study, GarA and SilM stock solutions (50 mg/mL each) were prepared using 1% carboxy-methyl cellulose (CMC) in sterile water. The stock solutions were prepared under aseptic conditions and autoclaved before use, to ensure sterility.

### 2.5 In vitro assays

### 2.5.1 Cell viability assay using resazurin

Cells were seeded in 96 well plate and allowed to adhere for 20 h, then treated with differentiation media for 3 days. Cells were treated with 10–100 µg/mL concentration of GarA, in increments of 10 µg/mL. After 24 h, the medium was aspirated and cells were washed with 1X PBS and new medium (100 µL) and resazurin was added (0.16 mg/mL, 10 µL) and the plate was incubated at 37  $^{\circ}\text{C}$  with 5%

 ${\rm CO_2}$  supply for 2 h. Later, the plate was read using a multimode reader for fluorescence at excitation 544 nm and emission 590 nm. No cell and no treatment control wells were kept for baseline correction and calculations of cell viability.

### 2.5.2 Reactive oxygen species estimation

Cells were seeded and treated similarly for differentiation, followed by GarA treatment (10  $\mu$ g/mL) with and without the presence of ethanol (500 mM) for 24 h. The concentration of 500 mM ethanol was selected based on preliminary cell viability assays (Supplementary Figure S2), which confirmed that SH-SY5Y cells remain sufficiently viable at this level over the experimental timeframe to allow for mechanistic analyses. Cells were incubated with DCFDA (2',7'-dichlorodihydrofluorescein diacetate) (10  $\mu$ M) for staining for 45 min, followed by lysis using Triton X 100 and measurement of fluorescent intensity at excitation 485 nm and emission 535 nm, using a multimode reader.

### 2.5.3 Observation of nuclear integrity using DAPI staining

Seeding, differentiation and treatment of GarA and ethanol were given similarly as previous section. After 24 h incubation, the cells were fixed using 4% fixing buffer and stained using DAPI (4',6-diamidino-2-phenylindole) (50 nM) for 15 min. Cells were washed using 1X PBS thrice and fluorescence intensity was measured at 355 nm excitation/ 460 nm emission. Images were captured using a fluorescence microscope using the blue channel.

### 2.6 In vivo study

### 2.6.1 Animal experimentation

After acclimatization, male Wistar rats were randomly divided into five groups: Isocaloric Control (NC), Ethanol-fed (E), Standard drug-SilM (50 mg/kg) (STD), GarA-low dose (50 mg/kg) (GAL) and GarA-high dose (100 mg/kg) (GAH), (Toppo et al., 2017), maintaining a similar average weight in each group. The control group was fed an isocaloric maltodextrin liquid diet, containing equal amounts of calories as compared to the ethanol fed groups, to rule out the variation caused due to caloric differences. While the remaining groups were fed ethanol containing Lieber-DeCarli diet (Supplementary Tables S2-S5). The concentration of maltodextrin and ethanol was increased gradually in 5 days, starting from 1% to 5% on the fifth day. The feeding protocol was continued for 30 days. To mimic normal drinking conditions, the rats were fed with 31.5% maltodextrin and ethanol on 11th and 22nd day (Liu et al., 2023) (Supplementary Table S6). No animals were excluded from the analyses, and the investigators performing further analyses were blinded (using coded identifiers known only to the personnel administering treatment) to the treatment groups.

### 2.6.2 Brain weight and histopathological observation

Brain samples were collected and weighed. Their size and appearance were noted and compared. Samples were stored in a 10% neutral buffered formalin solution for fixing. Samples were embedded in paraffin wax and washed for 2 h under running water. Blocks were then dehydrated using increasing concentration of

isopropyl alcohol (30%–70% – 90%–100%) and deparaffinized using xylene, and impregnated in melted paraffin wax. Thin sections (4–5  $\mu m)$  of the samples were cut using automated rotary microtome (Leica RM2255). The sections were fixed on poly-L-lysine coated (0.1% w/v in  $H_2O$ ) slides and stained using hematoxylin and counterstained with eosin using Gemini AS Automated Slide Stainer (Thermo Scientific). The stained slides were observed under a phase contrast microscope at  $\times 40$  magnification (Suvarna et al., 2012).

#### 2.6.3 Immunohistochemical observation

The tissues were fixed, and slides were prepared similarly as in case of HE staining. Sections were de-paraffinized and rehydrated. Autoclave method was utilized for antigen retrieval as per (Bankfalvi et al., 1994), containing antigen retriever buffer of pH 9.0, after a complete cycle of autoclave, the sections were incubated in the buffer for 2 min. Sections were cooled and washed using tris-buffered saline (TBS) pH 7.4, and quenching of endogenous peroxidase was carried out using incubation in 3%  $\rm H_2O_2$  for 30 min. The sections were then incubated in anti-vimentin V9 (Thermo scientific, MA5-11883, 1:200) primary antibody. Later, the sections were rinsed with TBS and incubated in EnVision Detection Systems, Peroxidase/DAB, Rabbit/Mouse (Agilent, Dako, Denmark) for 30 min at 25 °C. The sections were counterstained using Mayer's hematoxylin and mounted. Canine mammary tumor samples were used as positive controls (Wang et al., 2022).

### 2.6.4 Protein isolation and ELISA

The tissue samples were thawed, and 200 mg samples were taken. The samples were homogenized in 500  $\mu L$  RIPA buffer (prepared as per Ruiz-Uribe and Bracko, 2020) under ice incubation. After 2 h incubation at - 20 °C, samples were thawed and centrifuged at 12,000 rpm at 4 °C for 20 min. The upper aqueous layer was collected and used for ELISA estimation using specific kits for TNF $\alpha$ , BDNF, heme oxygenase 1 (HO-1), nuclear factor erythroid 2-related factor 2 (Nrf2), IL-6 and MCP-1, following the kits' protocol.

### 2.7 Gene expression study

SH-SY5Y cells were plated in six well plates and differentiated. After differentiation, cells were treated in four different groups: ethanol (500 mM), GarA (10 µg/mL), ethanol (500 mM) with GarA (10 µg/mL) and no treatment control for 24 h. Brain tissue samples were weighed (100 mg) and homogenized. RNA from both cells and tissue samples was isolated using RNA isoplus (Takara) and cDNA was prepared using kit method (Thermo Verso cDNA synthesis kit). To anticipate the neuroprotective effect of GarA against ethanol in cellular and rodent models, various genes were selected. For in vitro, genes for the neurotrophic factor BDNF, pro-inflammatory cytokines and chemokines such as TNFa and MCP-1, and antioxidant genes such as Nrf2 and HO-1, and lastly for the integrity of the BBB, Claudin1 (CLDN) was selected. And for in vivo, BDNF, vimentin, PCSK9, HO-1, Nrf2, interleukin 10 (IL-10), MCP-1, TNFα, and CLDN5 were selected. 18S (for in vitro) and βactin (for in vivo) were used as the housekeeping genes for the samples. The primers used were designed in silico using

PrimerBLAST (Ye et al., 2012) and have been published previously (Patel et al., 2021; Aghara et al., 2024; Chadha et al., 2025) (Supplementary Tables S7 and S8). For qPCR, SYBR green master mix and Agilent MxPro3000 were used.

# 2.8 Molecular docking and molecular dynamics (MD) simulations

Three target proteins: BDNF (PDB ID: 1BND)(Robinson et al., 1995), IL-6 (1ALU) (Somers, 1997), and MCP-1 (1DOL) (Lubkowski et al., 1997) were selected for docking analysis. Protein structures were retrieved from the RCSB Protein Data Bank and prepared using Schrödinger's Protein Preparation Wizard (Madhavi Sastry et al., 2013) (Maestro, v2024-2), including bond order assignment, hydrogen addition, hydrogen-bond optimization (PROPKA, pH 7.4), water removal (>5 Å from hetero groups), and restrained minimization with the OPLS4 force field (Lu et al., 2021) (RMSD cutoff: 0.3 Å). To compare the results of the docking interaction of GarA with the target proteins, docking with known binders of BDNF (4-methyl catechol) (Vetrivel et al., 2012), IL-6 (Pinostrobin chalcone) (Tjiptaningrum et al., 2024) and MCP-1 (Bindarit) (Paccosi et al., 2012), was performed. The threedimensional structures of GarA and known binders were downloaded from PubChem.

The receptor grid was generated using Glide's Receptor Grid Generation module (Friesner et al., 2006). The grid was centered on the binding sites of BDNF (Sangeet et al., 2023), IL-6 (Litov et al., 2021) and MCP-1 (Reid et al., 2006) and extended to cover a 20  $Å^3$  volume to allow full conformational sampling of the ligand. A van der Waals scaling factor of 1.0 and a partial charge cutoff of 0.25 were used for nonpolar atoms. No positional or hydrogen bond constraints were applied to retain unbiased binding predictions. Docking was carried out using Glide in Extra Precision (XP) mode, which incorporates a more discriminating scoring algorithm that includes terms for hydrophobic enclosure, desolvation penalties, ligand strain energy, and explicit treatment of directional hydrogen bonding. The best-ranked pose based on Glide XP score was selected for post-docking analysis and minimization. Key ligand-protein interactions were visualized using Maestro v12.5 and PyMOL 3.0.2.

To evaluate the stability and dynamic behavior of the protein-ligand complex, molecular dynamics (MD) simulations were performed using the Desmond module (Bowers et al., 2006) in Schrödinger Suite (version 2024-2). The docked complex obtained from XP docking was first imported into the System Builder panel, where it was embedded in an orthorhombic simulation box and solvated using the TIP3P explicit water model (Jorgensen et al., 1983). A buffer distance of 10 Å was maintained between the complex and the edges. The system was neutralized by adding appropriate counterions (Na<sup>+</sup> or Cl<sup>-</sup>), and 0.15 M NaCl was added to mimic physiological ionic strength. The OPLS4 force field was used for all protein, ligand, and solvent parameters. A series of energy minimizations were performed to eliminate bad contacts, followed by equilibration steps under NVT and NPT ensembles. The production MD simulation was

run for 100 ns under NPT ensemble conditions at 300 K temperature and 1.01325 bar pressure, maintained using the Nose-Hoover thermostat and Martyna-Tobias-Klein barostat, respectively (Nosé, 1984; Martyna et al., 1994). A time step of 2 fs was used, and trajectories were saved every 100 ps for analysis. Trajectory analysis included root mean square deviation (RMSD) root mean square fluctuation (RMSF), and ligand-protein interaction profiles over time, using the Simulation Interaction Diagram tool in Maestro. Additionally, the ligand-protein contacts throughout the trajectory were monitored to evaluate the stability and duration of binding interactions over the course of the simulation.

### 2.9 Network pharmacology

To identify probable protein targets of GarA, multiple web-based prediction tools were utilized, including PASS Online (Filimonov et al., 2014), TargetNet (Yao et al., 2016), SwissTargetPrediction (Daina et al., 2019), Similarity Ensemble Approach (SEA) (Keiser et al., 2007), and PharmMapper (Liu et al., 2010). All predicted targets were compiled, and duplicates were removed to generate a non-redundant list of GarA-associated proteins.

Genes associated with ethanol-induced brain damage were retrieved using the keywords "ethanol-induced brain injury" and "ethanol-induced brain damage" from the following databases: NCBI Gene, DisGeNET (Piñero et al., 2019), and GeneCards (Stelzer et al., 2016). All gene lists were standardized and merged, with duplicate entries eliminated.

The intersection between GarA targets and ethanol-related disease genes was determined using Venn diagram analysis (Venny 2.1.0) (Oliveros, 2015) to identify common targets potentially relevant to neuroprotection. These overlapping genes were submitted to the STRING database (Szklarczyk et al., 2023) (confidence score >0.4) to construct a protein–protein interaction (PPI) network. The resulting PPI data were imported into Cytoscape (v3.9.1) (Shannon et al., 2003) for network visualization and analysis, including topological parameter calculation.

To explore the functional significance of the overlapping genes, the top 20 core genes were submitted for Gene Ontology (GO) (biological process, molecular function, cellular component) and Kyoto Encyclopaedia of Genes and Genomes (KEGG) pathway enrichment analyses were performed using ShinyGO v0.77 (Ge et al., 2020). Terms with a p-value <0.05 were considered statistically significant. Enrichment results were visualized as bar plots and bubble charts.

#### 2.10 Statistical analysis

Cell culture assays were performed in biological triplicates (n = 3), while animal experimentation was carried out in six biological replicates (n = 6). For histological analyses, multiple fields per animal were quantified, and the average per animal was used as the experimental unit for statistical analysis. Data were expressed as Mean  $\pm$  SD, where a value of p < 0.05 was considered significant. Statistical analyses were performed using GraphPad Prism

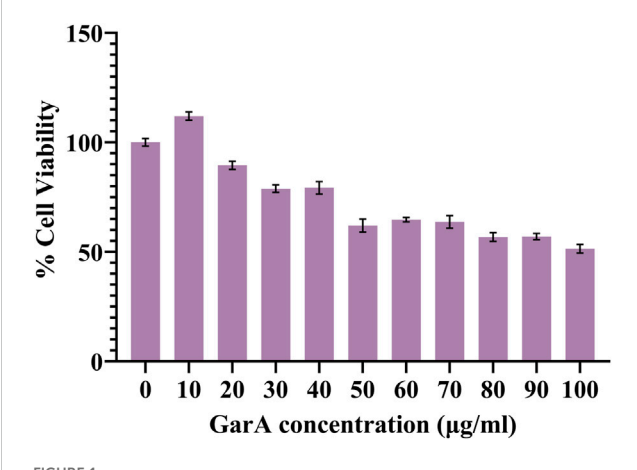


**FIGURE 1** Cell viability of SH-SY5Y cells in presence of GarA (10–100 µg/mL). Data was normalized by control and represented as Mean  $\pm$  SD. Significance was calculated using One-way ANOVA with Dunnet's multiple comparisons, where the significance between 0, 10 and 20 µg/mL was p > 0.05, whereas 0, 30 and 40 µg/mL was p < 0.01 and 0 and 50–100 µg/mL was p < 0.0001 (n = 3).

9.1.0 and involved One-way analysis of variance (ANOVA) with either Dunnet's or Tukey's HSD post-hoc multiple comparisons test.

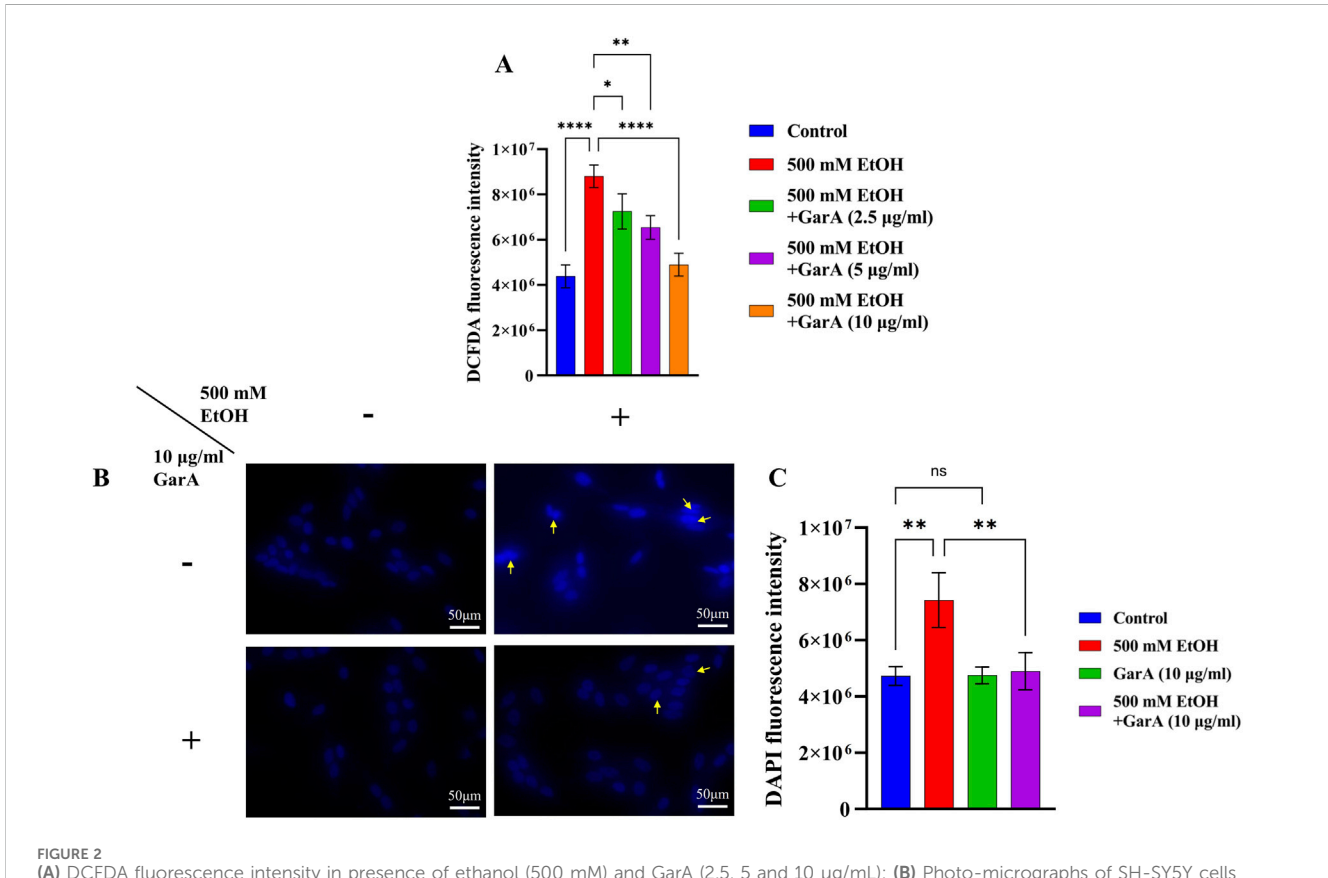
### 3 Results

# 3.1 GarA confers neuroprotection in SH-SY5Y cells

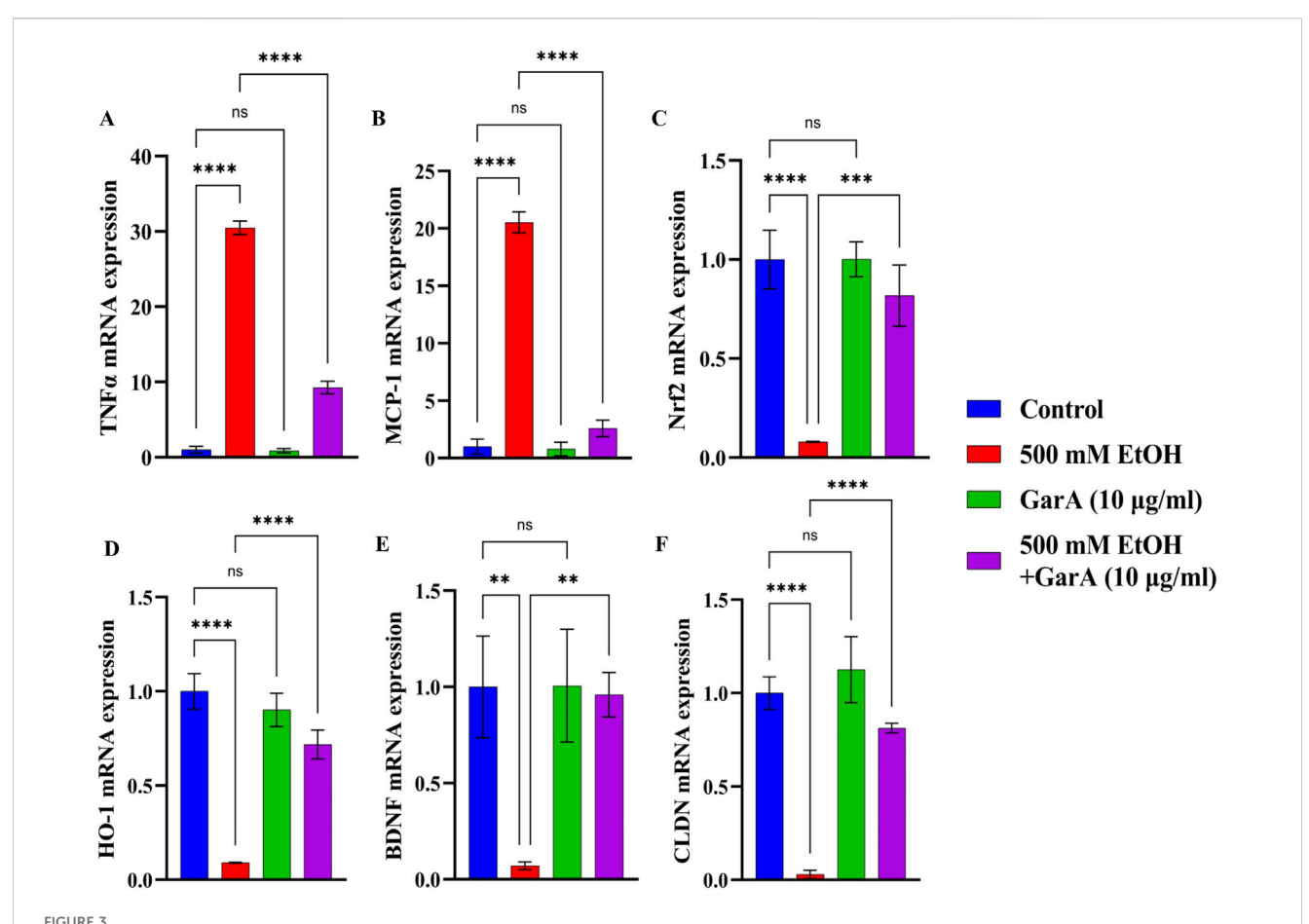
The resazurin assay was performed to evaluate the effect of GarA on the neuroblastoma cell line, SH-SY5Y. Cells showed a dose-dependent decrease in cell viability (Figure 1). Maximum viability was observed at 10  $\mu$ g/mL GarA, which showed more than 100% viability, showing maintained or slightly enhanced cell viability relative to control. This assay showed that GarA is less toxic till 40  $\mu$ g/mL, and shows a cell viability above 75%. The lowest viability was observed at a concentration of 100  $\mu$ g/mL (~50%).

# 3.2 GarA mitigates ethanol-induced oxidative stress and nuclear damage in SH-SY5Y cells

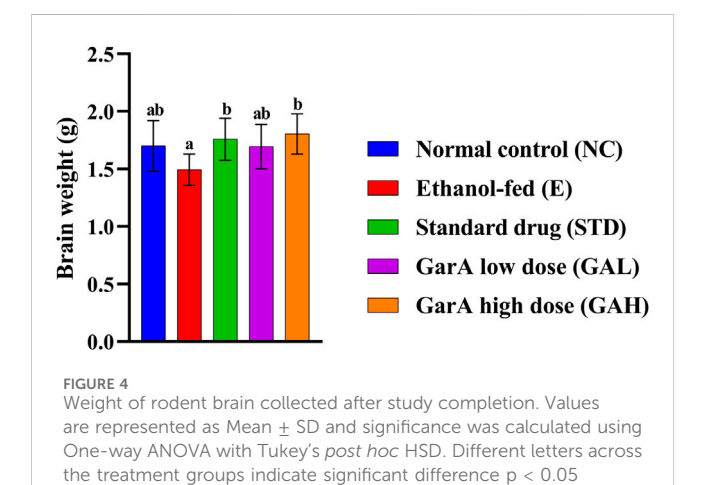
The ROS and nuclear damage caused due to ethanol treatment, and its prevention using co-treatment with GarA was measured using DCFDA and DAPI staining methods. GarA showed protective effect against the ethanol induced oxidative damage, which was evident by a decrease in the



(A) DCFDA fluorescence intensity in presence of ethanol (500 mM) and GarA (2.5, 5 and 10  $\mu$ g/mL); (B) Photo-micrographs of SH-SY5Y cells (at x40 magnification) in presence and absence of ethanol (500 mM) and GarA (10  $\mu$ g/mL); (C) DAPI fluorescence intensity. Values are represented as Mean  $\pm$  SD and significance was calculated using One-way ANOVA with Dunnet's multiple comparisons where  $^{ns}p > 0.05$ ,  $^{*}p < 0.05$ ,  $^{*}p < 0.05$ ,  $^{*}p < 0.01$  and  $^{****p} < 0.0001$ . (n = 3) (Scale bar = 50  $\mu$ m).



GarA helps reduce inflammation and has an antioxidant and neuroprotective activity in SH-SY5Y cells against ethanol. Gene expression over 18S in vitro in different treatment groups showing (A). TNF- $\alpha$  (B). MCP-1 (C). Nrf2 (D). HO-1 (E). BDNF (F) CLDN. Values are represented as Mean  $\pm$  SD and significance was calculated using One-way ANOVA with Dunnet's multiple comparisons where  $^{ns}p > 0.05$ , \*p < 0.05, \*p < 0.01, \*\*p < 0.01 and \*\*\*p < 0.001 (n = 3).



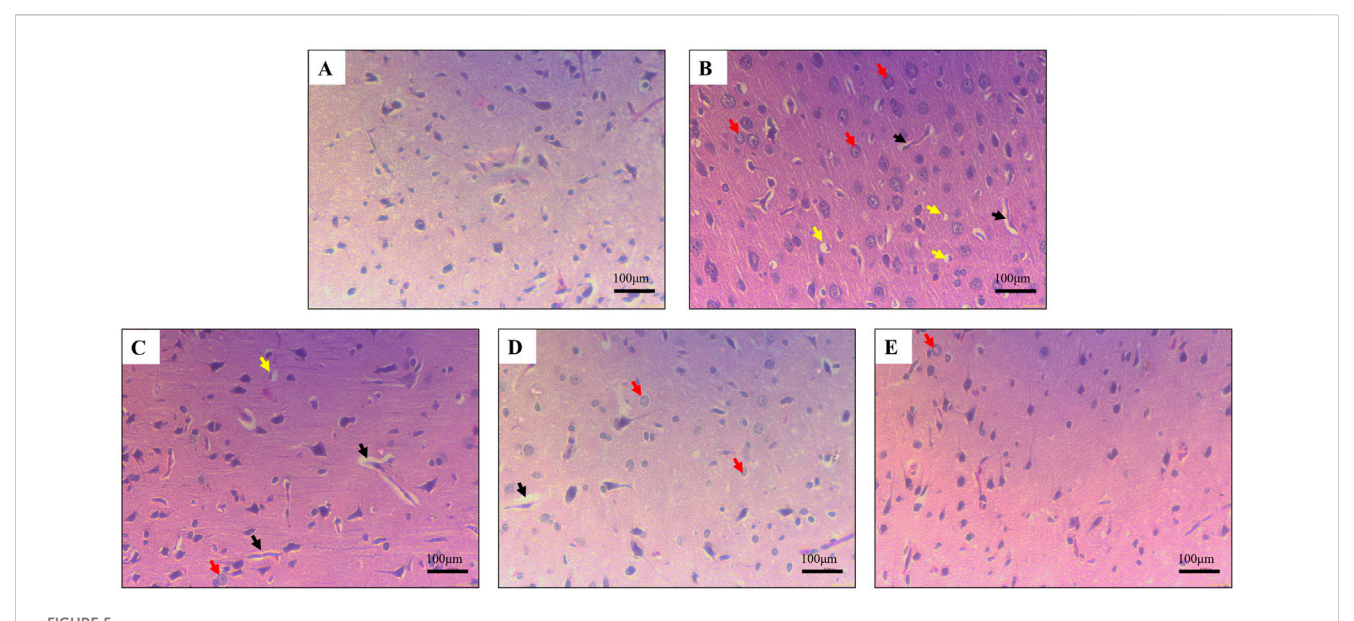
DCFDA fluorescence intensity in the co-treatment group, in comparison to the ethanol treatment alone. The cells in the untreated group and the GarA group showed a similar intensity (Figure 2A).

(n = 6)

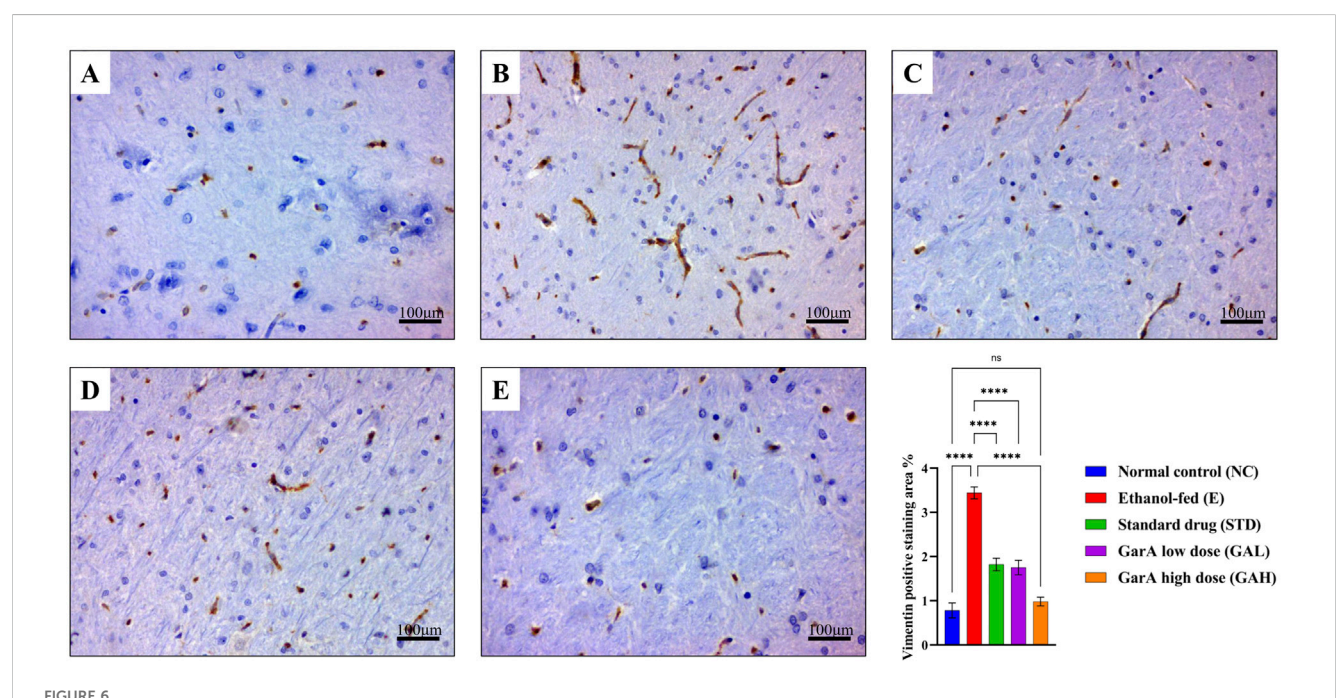
Likewise, the cells showed an uptake of higher amount of DAPI stain in the ethanol treated group. Additionally, the nuclei of that group showed an irregular or fragmented morphology accompanied by nuclear condensation (Figure 2B). The cells in the control, GarA alone and the co-treatment group showed more stable and protected nuclei in comparison to the ethanol group. This trend was observed in the fluorescence intensity of the groups (Figure 2C).

# 3.3 GarA modulates neuroprotective, inflammatory, and barrier-related gene expression *in vitro*

The gene expression study in SH-SY5Y cells showed neuroprotective effects of GarA via modulation of various genes. GarA aided in protection of the cells against ethanol induced inflammation, which was evident by a downregulation in the levels of TNF $\alpha$  and MCP-1, respectively, as compared to the ethanol alone treatment (Figures 3A,B). Additionally, GarA showed an increase in the expression of Nrf2 and HO-1, in the co-treatment group, as compared to the ethanol alone treatment group (Figures 3C,D). The expression of BDNF in the GarA (1.00  $\pm$ 



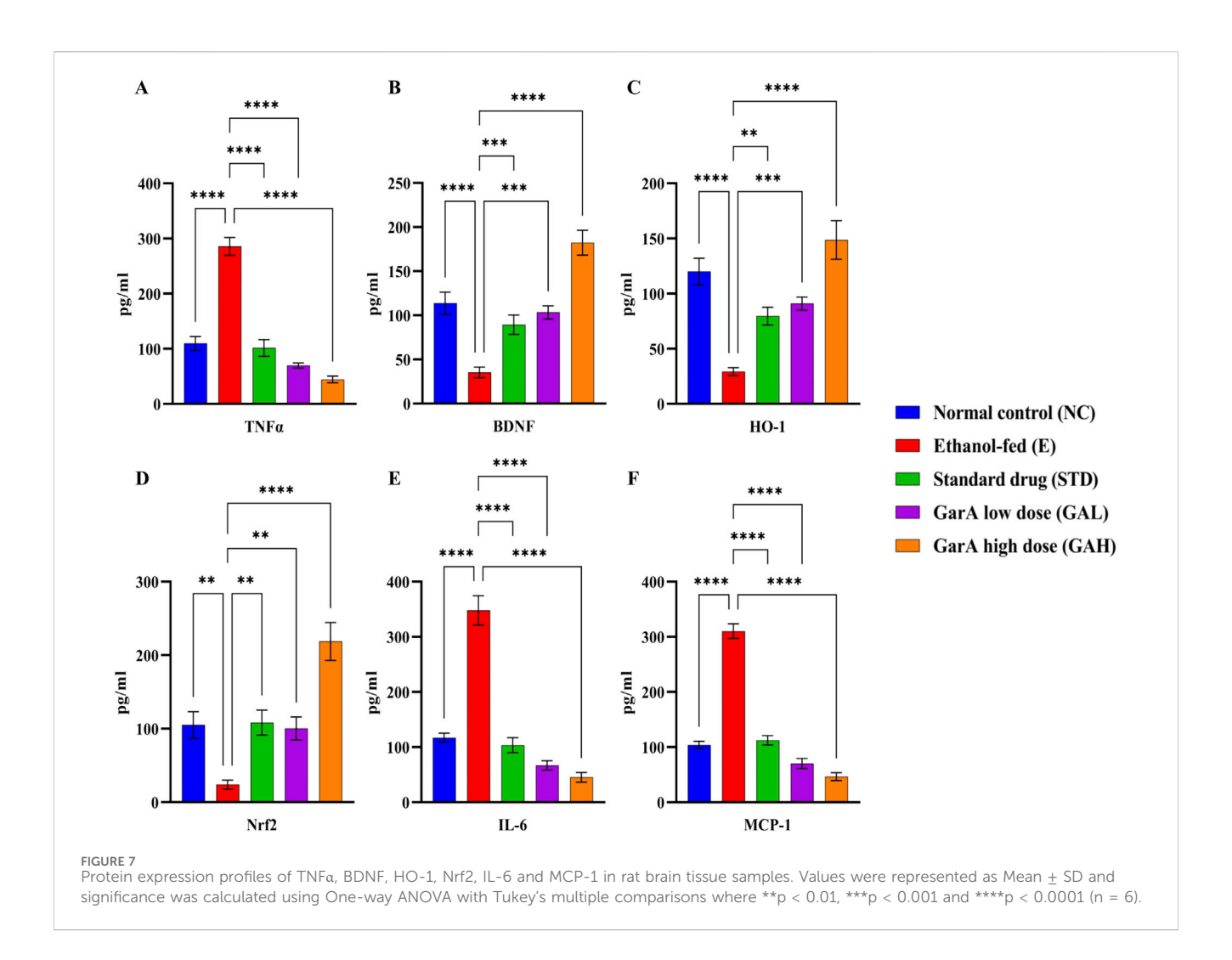
Haematoxylin and eosin staining in rat cerebral cortex showing (A) normal morphology in control (B) damaged neuronal morphology in ethanol-fed rodents (C) and (D) slightly improved neuronal morphology in Standard drug treated and GarA low dose (GAL), respectively (E). Improved neuronal tissue and cells in GarA high dose (GAH) treated rodents. Black arrows depict vacuolisation, yellow arrows show pericellular space around necrotic neurons and red arrows show pyknotic nuclei. Images taken at ×40 magnification and scale bar depicts 100 µm.



Vimentin immunohistochemistry for staining reactive astrocytes. Photo-micrographs of rat brain cerebral cortex at  $\times$ 40 magnification stained using anti-vimentin antibody showing **(A)** normal in control **(B)** increased positive staining in ethanol-fed rats and decreased in **(C)** drug treated **(D)** low dose GarA and **(E)** high dose GarA treated rats **(F)**. Graph showing vimentin positive staining area % in different groups (fields/animal). Values are represented as Mean  $\pm$  SD and significance was calculated using One-way ANOVA with Tukey's post hoc HSD where "sp > 0.05, and \*\*\*\*p < 0.0001 (n = 6, technical replicates).

0.293) and co-treatment groups (0.96  $\pm$  0.115), were comparable to the control group (1.00  $\pm$  0.264) ( $^{ns}p >$  0.05), and markedly higher as compared to the ethanol treated cells (0.07  $\pm$  0.020) (Figure 3E).

Moreover, the co-treatment with GarA (0.81  $\pm$  0.025) caused an upregulation in the expression of CLDN, in comparison to the ethanol group (0.03  $\pm$  0.022) (Figure 3F).



## 3.4 GarA attenuates ethanol-induced brain injury and inflammation in vivo

### 3.4.1 GarA preserves brain architecture and astrocyte activation status

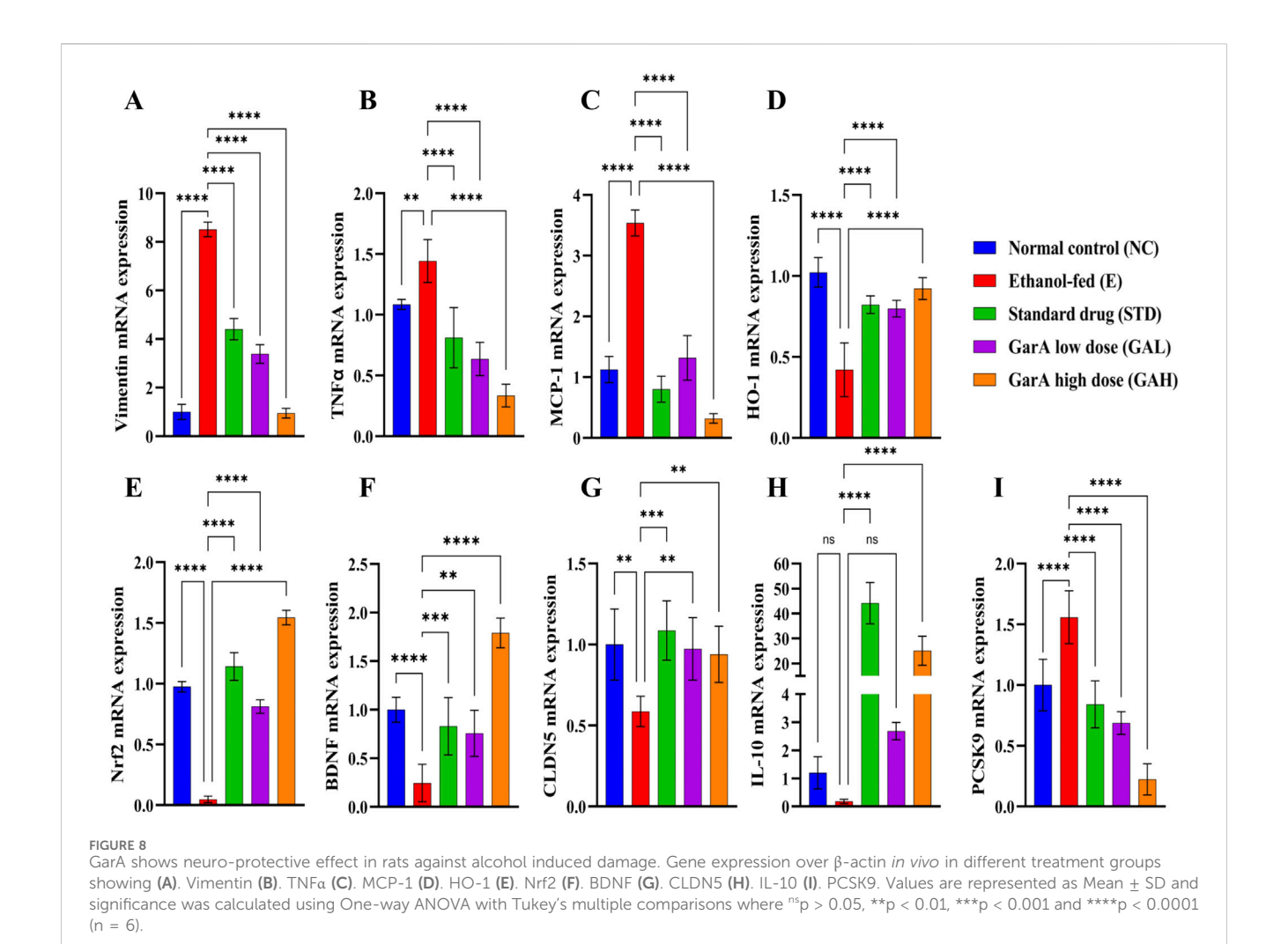
Chronic alcohol consumption can cause neuronal loss which leads to a decrease in the brain size and weight (Crews, 2008). The rats receiving SilM (STD group), or GarA treatment showed bigger brain sizes, and higher weight (Figure 4) as compared to the disease group. Moreover, the HE staining showed more normal morphology of neurons in the control (100%) and GAH (96.1%) groups, in comparison to the disease group (71.7%) (Figure 5). While the STD and GAL group showed a few anomalies, the morphology appeared improved as compared to the disease group. The neurons in the disease group showed pyknosis (16.6%), formation of vacuoles (5.7%) and pericellular spaces (5.7%) around the necrotic neurons (Ghosh et al., 2021). This trend was decreased in case of STD and GAH groups, where only 2.2% pyknosis was observed in each of those groups. Vimentin is a marker of astrocyte activation and reactive gliosis leading to neurodegeneration (Zhang et al., 2025). Through immunohistochemistry experiment, it was observed, that the brain tissue of the disease group showed increased staining with vimentin, showing higher neuronal activation. This pattern changed, and a decrease in the vimentin uptake was observed in the GAH group (Figure 6). Similarly, the gene expression levels of Vimentin in rat brain tissue showed a similar trend (Figure 8A).

# 3.4.2 GarA helps in neuroprotection against alcohol induced damage in rats

Protein expression in rat brains was estimated using ELISA kits for selected protein targets. TNF $\alpha$  in the diseased group (E), was found to be upregulated 3-folds of the control (NC) rats. While it was observed that the expression decreased in the STD and GarA treated groups. Moreover, the expression of BDNF showed an upregulation in the case of GAH animals, as compared to the NC animals as well. BDNF was diminished in the disease (E) group. Similar trends were observed in the expression of HO-1 and Nrf2 expression profiles, further corroborating the results. Notably, it was observed that for IL-6 and MCP-1, the GAH group showed a drastic reduction in the expression, as compared to all the other groups (Figure 7).

# 3.4.3 GarA regulates gene expression associated with neuroinflammation and barrier function in rat brain

Alcohol consumption causes inflammation, alters brain function and decreases the BBB integrity (Vore and Deak,



2022). Gene expression study carried out using rat brain tissue showed an ethanol-induced increase in TNF $\alpha$  levels in the disease group (1.44  $\pm$  0.176), which was decreased in the GAH group (0.33  $\pm$  0.092), even less than the control group (1.08  $\pm$  0.041) (Figure 8B). Likewise, the chemokine MCP-1 (CCL-2), was upregulated in the disease group (3.54  $\pm$  0.213) and downregulated in the GAH group (0.32  $\pm$  0.077) (Figure 8C). On the contrary, the GAH group showed an upregulation in the expression of HO-1 and Nrf2 levels, as compared to the disease group (Figures 8D,E).

Additionally, the factor for neuronal growth, development and survival, BDNF, was found to be upregulated 2-fold in the GAH group (1.79  $\pm$  0.152) as compared to the control group (1.00  $\pm$  0.012). While the disease group (0.24  $\pm$  0.192) showed an approximate 4-fold decrease in the expression as compared to the control group. Expression for the STD and GAL groups, was comparable to control, but less than the GAH group (Figure 8F).

Furthermore, it was observed that SilM and GarA treatment showed an increase in CLDN5, meaning increased BBB integrity. Contrastingly, the disease group and low dose treatment (GAL) groups showed a decreased expression, hence increased permeability due to the barrier junction dysfunction caused by ethanol (Figure 8G). Notable increase in IL-10 expression in the GAH

group was observed, similar to the SilM treated standard group (Figure 8H). Whereas, the PCSK9 expression was decreased drastically in the GAH group and upregulated in the ethanol fed rodents (Figure 8I).

# 3.5 Molecular docking and MD simulations reveal stable complex formation of GarA with BDNF, IL-6, and MCP-1

### 3.5.1 GarA shows binding in the active site of BDNF, IL-6 and MCP-1

Molecular docking analysis demonstrated that GarA binds effectively in the active sites of BDNF, IL-6, and MCP-1 through a range of stabilizing interactions. In the BDNF–GarA complex (Figure 9), GarA engaged in multiple conventional hydrogen bonds with key residues ARG88 and TYR52 with a binding energy of –4.17 kcal/mol. The complex also had van der Waals and hydrophobic interactions involving TRP19, VAL42, VAL44, LEU49, PHE53, VAL87, ALA89, TRP100 and PHE102. The binding was further stabilized by charged positive interactions with LYS50 and ARG88, and polar interaction with GLN51, highlighting a robust interaction interface. In the IL-6–GarA

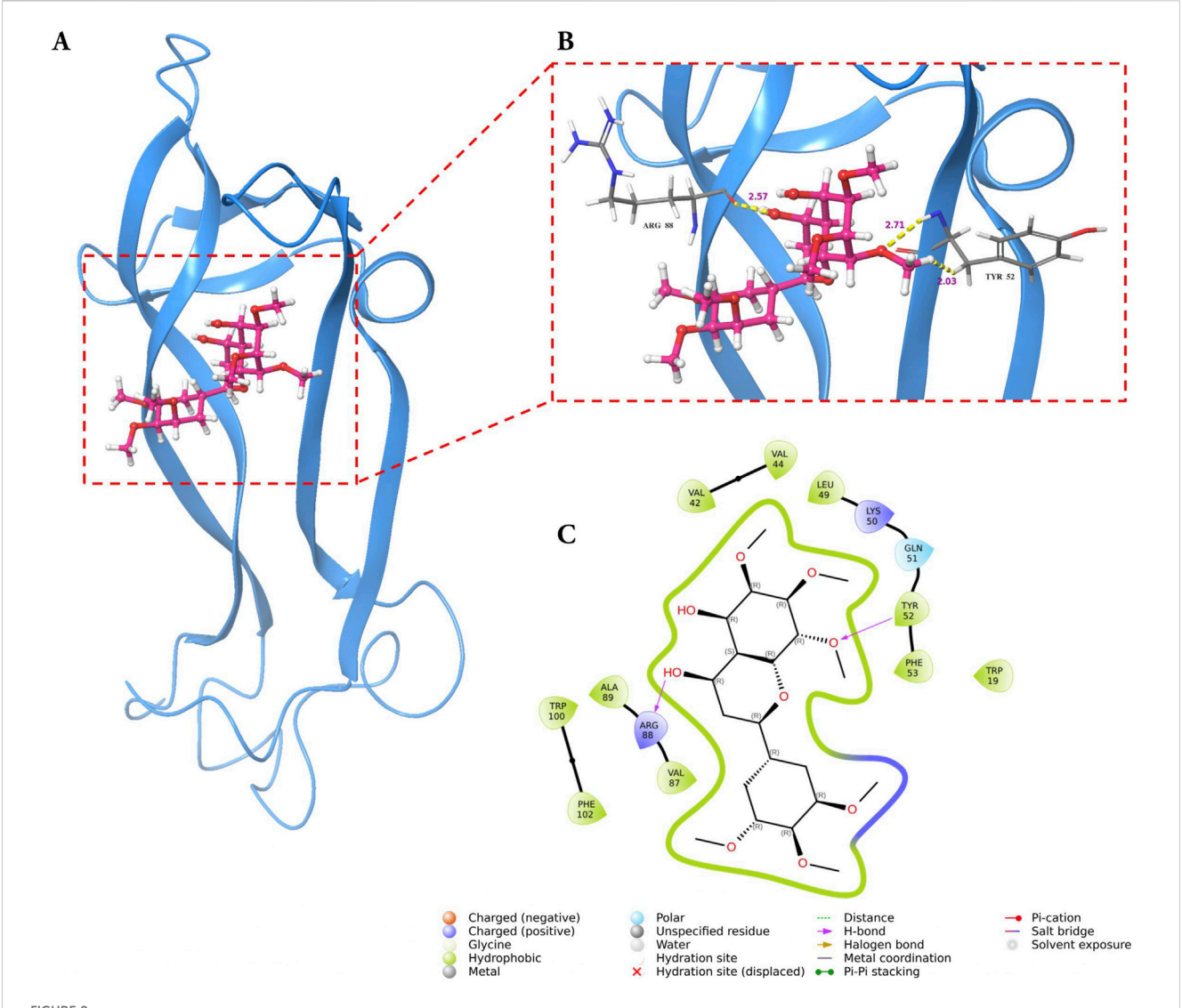


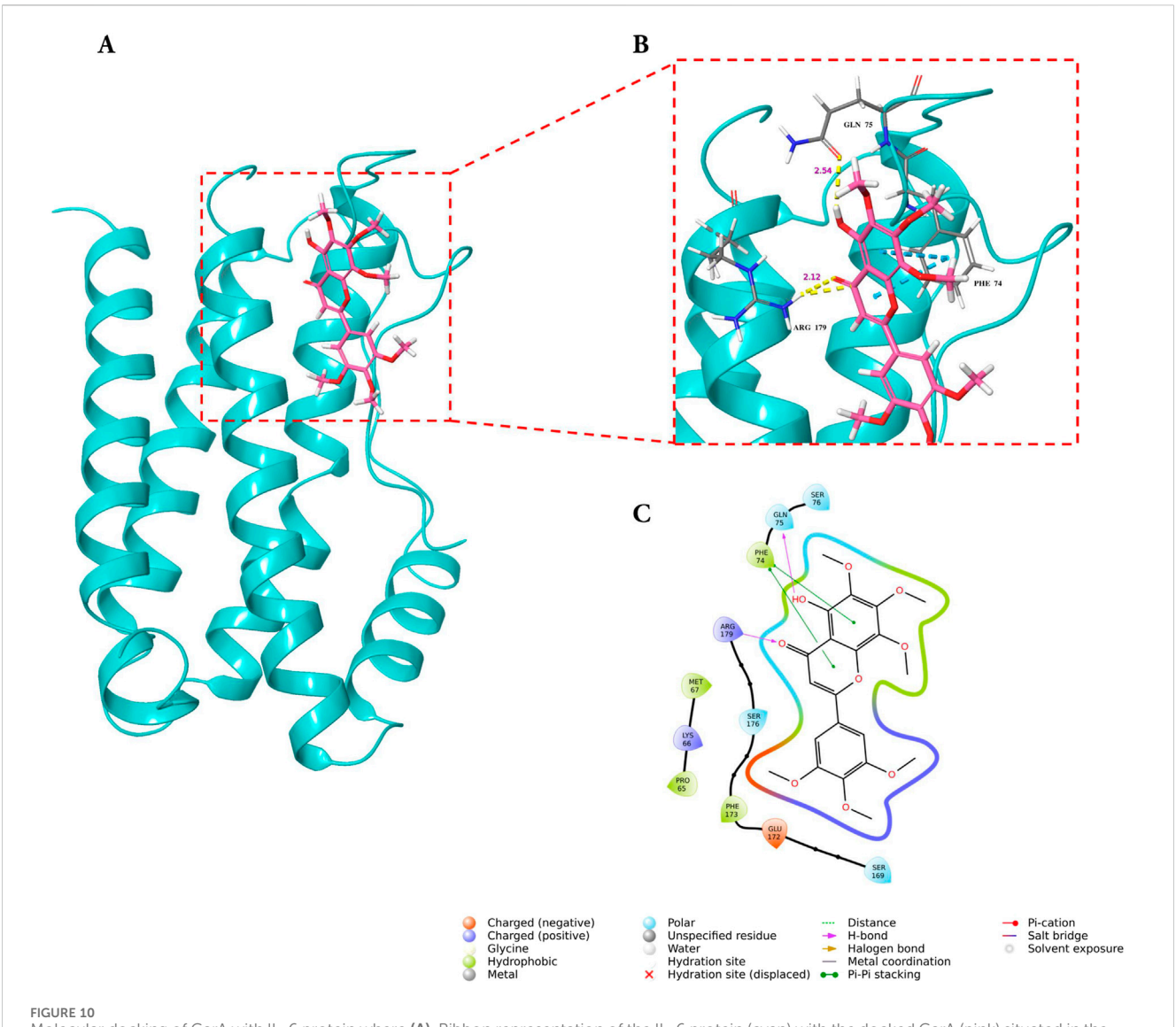
FIGURE 9

Molecular docking of GarA with BDNF protein where (A). Ribbon representation of the BDNF protein (blue) with the docked GarA (pink) situated in the hydrophobic binding cavity, (B). Zoomed-in view of the binding site showing key hydrogen bonding interactions between the ligand and active site residues including TYR52 and ARG88. Distances (in Å) represent favourable hydrogen bonding geometry, and (C). 2D ligand interaction diagram, illustrating hydrogen bonds, hydrophobic contacts, and surrounding residues.

complex (binding energy = -3.23 kcal/mol) (Figure 10), GarA exhibited strong hydrogen bonding with ARG179 and GLN75, as well as charged negative contact with GLU172 and positive contacts with LYS66 and ARG179. Polar contacts with GLN75, SER76, SER169 and SER176, also contributed to the stable bonding. Notably,  $\pi$ - $\pi$  stacking with PHE74 and hydrophobic bonding with PRO65, MET67, PHE74 and PHE173, supported additional stabilization. The MCP-1-GarA (Figure 11) complex showed a binding energy of -4.63 kcal/mol supported by hydrogen bonding with TYR13 and ASN14, and hydrophobic interactions with CYS11, CYS12, PHE15, ILE49, ILE51 and CYS52. Polar interactions were also prominent, especially involving THR10, and THR16. These molecular interactions indicate favorable binding conformations across all three protein targets as compared to known ligands, with comparable binding energies and interacting residues (Supplementary Table S9).

## 3.5.2 MD simulations show stable complex formation of GarA with molecular targets

To further validate the stability of GarA within the protein-ligand complexes, 100 ns molecular dynamics simulations were conducted for BDNF, IL-6 and MCP-1. For the BDNF–GarA complex (Figure 12A), RMSD remained stable around 3.0 Å, and fluctuations were minimal in the structured domains. The ligand RMSD remained under 2.0 Å, with stable hydrogen bonds formed with TYR52 and ARG88. Water bridges with LYS50, TYR52, TYR54 and ARG88 further contributed to ligand affinity, supporting a potential modulatory role of GarA on neurotrophic signalling. The IL-6–GarA complex (Figure 12B) also displayed equilibrium RMSD profiles, with minimal drift and ligand retention within the pocket. Key interactions with MET67, PHE74, GLN75, and ARG179 were observed, involving both hydrophobic contacts and hydrogen bonding. Water-mediated bridges contributed to transient stabilization, reinforcing the interaction



Molecular docking of GarA with IL-6 protein where (A). Ribbon representation of the IL-6 protein (cyan) with the docked GarA (pink) situated in the hydrophobic binding cavity, (B) Zoomed-in view of the binding site showing key hydrogen bonding interactions between the ligand and active site residues including PHE74, GLN75, and ARG179. Distances (in Å) represent favourable hydrogen bonding geometry, and (C). 2D ligand interaction diagram, illustrating hydrogen bonds, hydrophobic contacts, and surrounding residues.

profile. The MCP-1–GarA complex (Figure 12C) showed consistent protein backbone RMSD (3.0 Å) with a mild shift at later simulation stages (~4.5 Å), suggesting local conformational flexibility. Ligand RMSD was stable (<2.5 Å), with residues TYR13 and ASN14 exhibiting persistent hydrogen bonding. Additional hydrophilic and hydrophobic contacts were formed with GLU50, ARG29, and CYS52, stabilizing the ligand within the active site (Supplementary Figures S3-S5 and Supplementary Videos 1-3).

# 3.6 Network pharmacology reveals key targets and pathways of GarA in ethanol-induced brain injury

A total of 155 GarA-predicted targets and 1,239 ethanolassociated disease genes were retrieved. After eliminating duplicates, 107 intersecting genes were identified as common to both datasets (Figure 13A). The 107 intersecting genes were input into STRING to generate a PPI network, resulting in a graph with 107 nodes and 1,557 edges, and an average node degree of 29.1, which suggests higher protein interaction (Figure 13B). Genes with darker coloration indicated stronger interaction potential (Figure 13C). Visualization in Cytoscape and analysis via CytoHubba yielded the top 10 core hub genes based on degree centrality (Figure 13D). Similarly, given the role of tight junctions in BBB integrity, a tight junction-specific PPI network was constructed and merged with the GarA-target network. The resulting interaction map highlighted significant overlap, suggesting GarA may influence tight junction-related targets (Figure 14A).

Gene Ontology (GO) analysis of the top core genes revealed enrichment in biological processes such as response to oxidative stress, cytokine activity, and apoptotic regulation (Figures 14B–D).

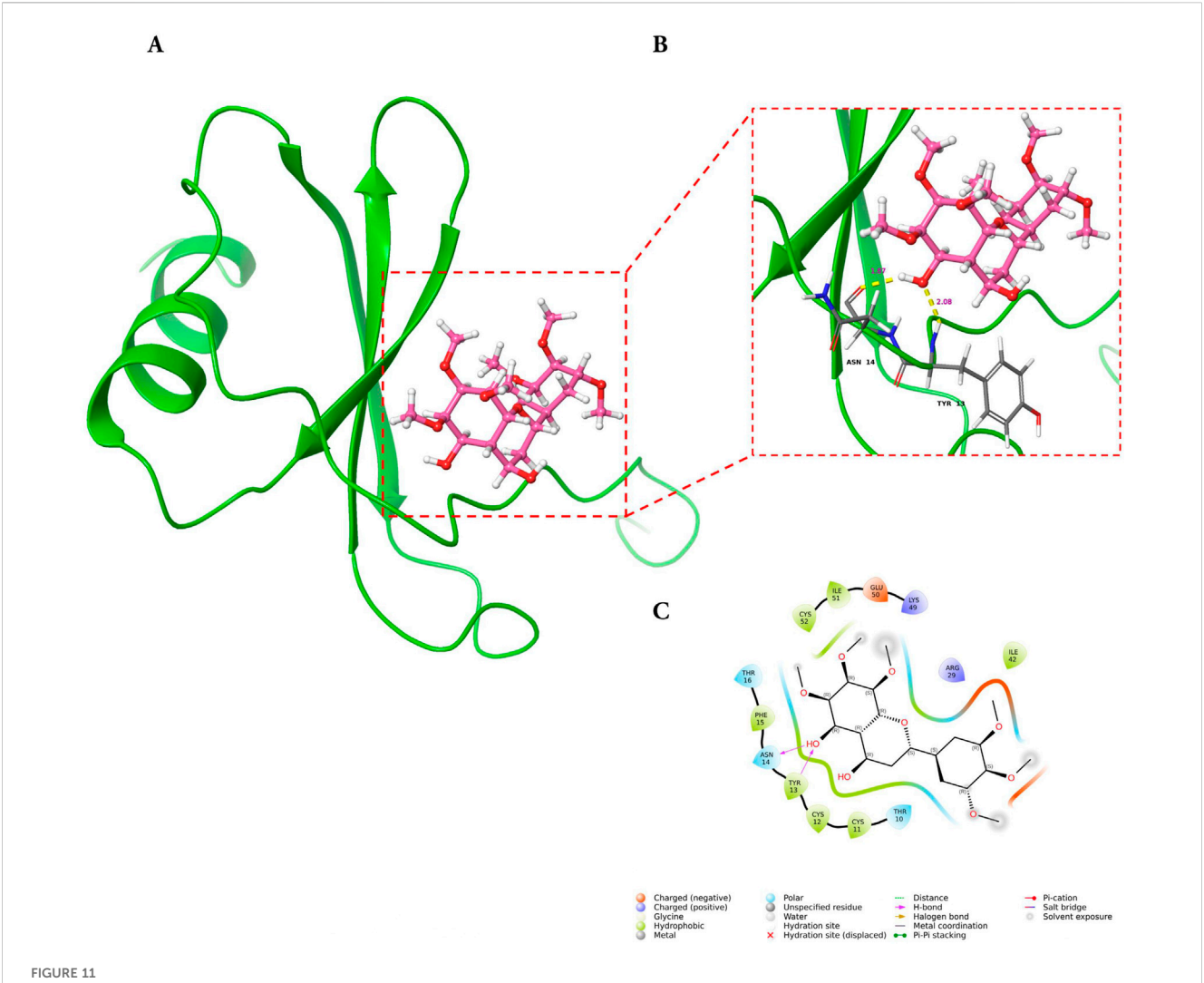


FIGURE 11
Molecular docking of GarA with MCP-1 protein where (A). Ribbon representation of the MCP-1 protein (green) with the docked GarA (pink) situated in the hydrophobic binding cavity, (B) Zoomed-in view of the binding site showing key hydrogen bonding interactions between the ligand and active site residues including TYR13, and ASN14. Distances (in Å) represent favourable hydrogen bonding geometry, and (C). 2D ligand interaction diagram, illustrating hydrogen bonds, hydrophobic contacts, and surrounding residues.

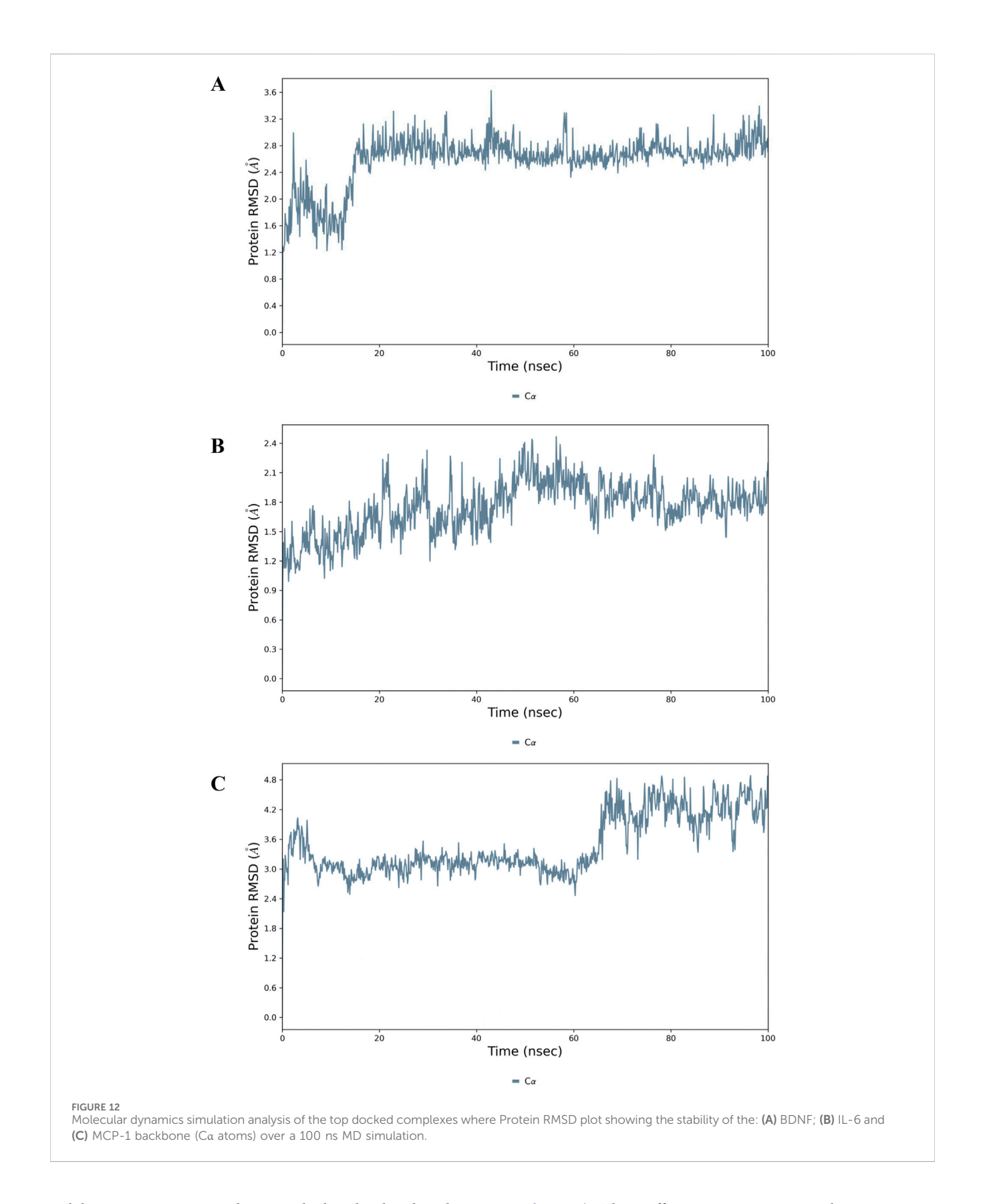
KEGG pathway analysis highlighted the association of GarA with pathways involved in tight junction integrity, TNF $\alpha$  signalling, IL-6, IL-17, HIF-1, and apoptosis (Figure 14E). Among these, the TNF $\alpha$  pathway emerged as a central node, linking oxidative stress, inflammation via IL-6, and BBB dysfunction, which are hallmark features of ethanol-induced neurotoxicity. A few of these predicted targets and pathways such as TNF $\alpha$ , BDNF, and Nrf2/HO-1 signaling, were consistent with the changes observed at the molecular level in the *in vitro* and *in vivo* assays in the current study, thereby reinforcing the biological relevance of the network pharmacology findings.

### 4 Discussion

Chronic ethanol consumption disrupts brain physiology via oxidative stress, glial reactivity, and impaired neurotrophic signaling (Fadda, 1998; Das et al., 2007; Yang and Luo, 2015;

Guerri and Pascual, 2019; Li et al., 2020). Sustained ethanol exposure leads to the activation of microglia and astrocytes, resulting in the release of inflammatory cytokines such as TNF $\alpha$ , IL-1 $\beta$ , and MCP-1 (Fernandez-Lizarbe et al., 2009; Zou and Crews, 2012; Pascual et al., 2015; Holloway et al., 2023). These proinflammatory mediators exacerbate neuronal damage, disturb synaptic communication, and facilitate neurodegenerative cascades that are implicated in disorders like AD and PD. (Kamal et al., 2020). Despite FDA-approved therapies for alcohol dependence, their impact on systemic health and long-term neuroprotection remains limited (MacKillop et al., 2022). Accordingly, the present study investigates the potential of GarA to prevent alcohol-induced brain damage.

GarA, a polymethoxylated isoflavone previously isolated and characterized (Chadha et al., 2025), was evaluated in this study for its neuroprotective potential. This is the first instance where GarA is investigated for its protective role against ethanol-induced neurotoxicity. In SH-SY5Y cells, GarA significantly enhanced cell



viability up to 40  $\mu$ g/mL and mitigated ethanol-induced oxidative stress by reducing intracellular ROS and stabilizing nuclear morphology. The ROS and DNA damage are caused due to elevated oxidative stress and pro-inflammatory cytokines (Haorah

et al., 2005). These effects were consistent with prior reports demonstrating the efficacy of GarA in reducing oxidative damage and inflammation in hepatic and intestinal cell models (Chadha et al., 2025) and EL-4 cells (Yang et al., 2020). In the current study,

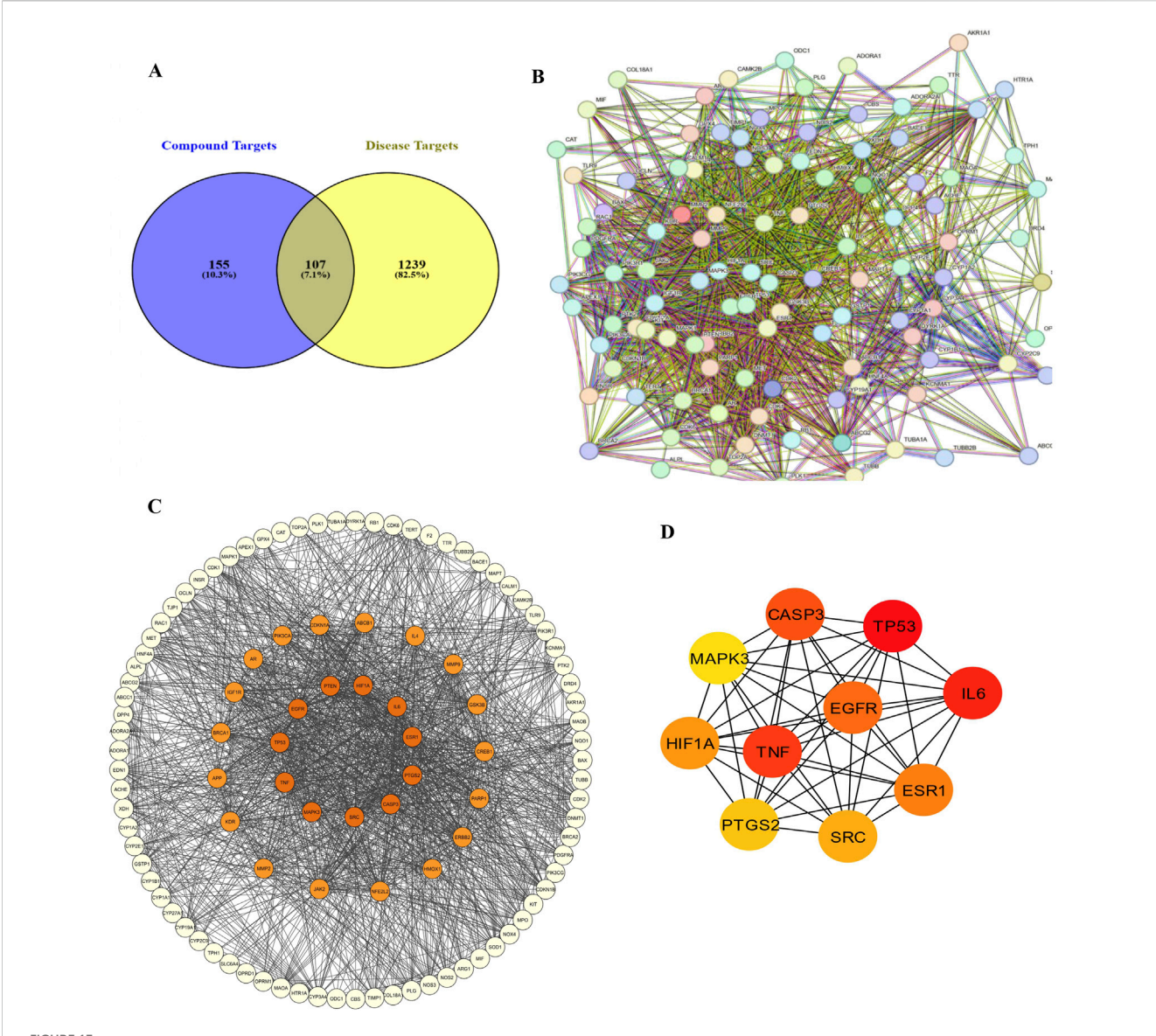


FIGURE 13

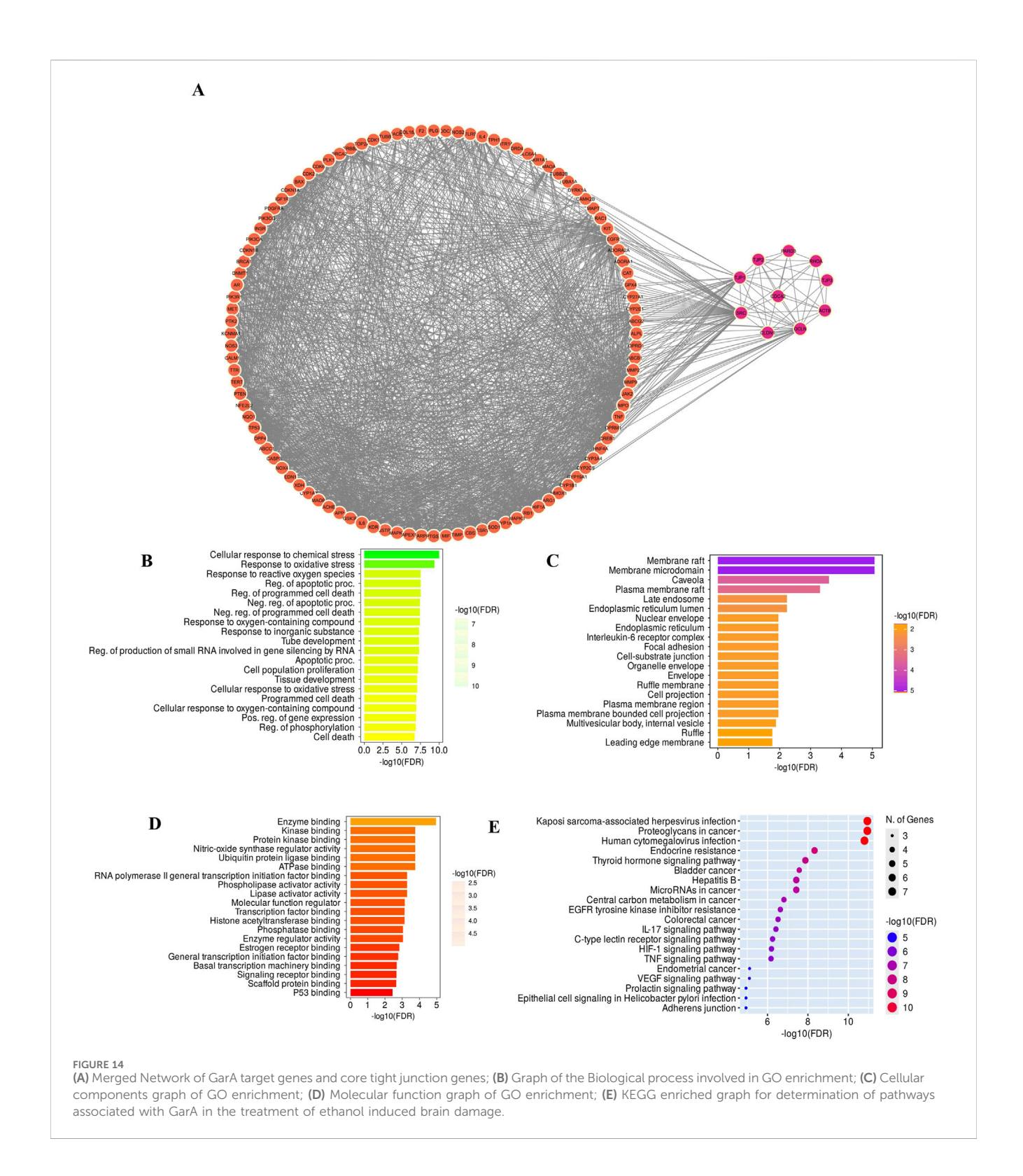
Network pharmacology between Gardenin A and ethanol induced brain damage: (A) Venn diagram of Gardenin A target genes and disease-related genes; (B) PPI network diagram; (C) Network of Gardenin A target genes in Ethanol-induced brain damage; (D) Top 10 core target genes of Gardenin A in disease

GarA treatment was associated with decreased pro-inflammatory cytokine levels and an increased expression of antioxidant genes, indicating a protective effect against ethanol-induced cellular damage.

Ethanol consumption in higher amounts leads to reduced brain weight (Das et al., 2007). GarA also exhibited protective effects *in vivo*. Ethanol-fed rodents demonstrated reduced brain weight and significant histoarchitectural alterations, including glial activation and pyknotic nuclei. Although brain concentrations of GarA were not directly measured, its lipophilic nature and previously reported ability to cross the BBB (Hack et al., 2024) suggest that it can access neuronal tissue at biologically relevant levels, supporting the plausibility of the observed *in vivo* neuroprotective effects. This also enables direct modulation of neuronal health and synaptic plasticity. GarA ameliorated neuronal damage and restored normal

brain histology. Previously, curcumin showed similar effects in histopathological morphology against rotenone induced PD (Fikry et al., 2022).

Beyond cellular oxidative damage, ethanol also affects neurovascular integrity, particularly the BBB, which is vital for maintaining brain homeostasis. The ROS generated due to ethanol disrupts the BBB due to activation of the myosin light chain kinase (MLCK) and disruption of tight junctions (Haorah et al., 2005; 2007a; 2007b). Here, GarA treatment was associated with preservation of BBB integrity, including modulation of CLDN5 gene expression. It also showed a promising antioxidant effect by causing a rise in the gene and protein levels of HO-1 and Nrf2, while decreasing the pro-inflammatory gene levels. As BBB breakdown allows infiltration of inflammatory mediators and immune cells, it also facilitates the activation of resident glial



cells, further amplifying neuroinflammation. While we quantified neuronal damage and glial activation, BBB integrity using protein expression studies was not assessed in the present study. Future work, including quantitative evaluation of tight junction proteins such as CLDN5 will be important to further validate the neuroprotective effects of GarA. Given the upregulation of Nrf2 and HO-1, GarA may exert its antioxidant effects via

activation of the Nrf2 signaling pathway, a central mediator of cellular responses to oxidative stress (Qiao et al., 2024). Previous studies have implicated phytochemicals in modulating this pathway (Feng et al., 2022), which could explain the enhanced antioxidant enzyme expression observed in the current model.

Neuroinflammatory reactivity, particularly through  $TNF\alpha$  and glial activation, was evident in both gene and protein

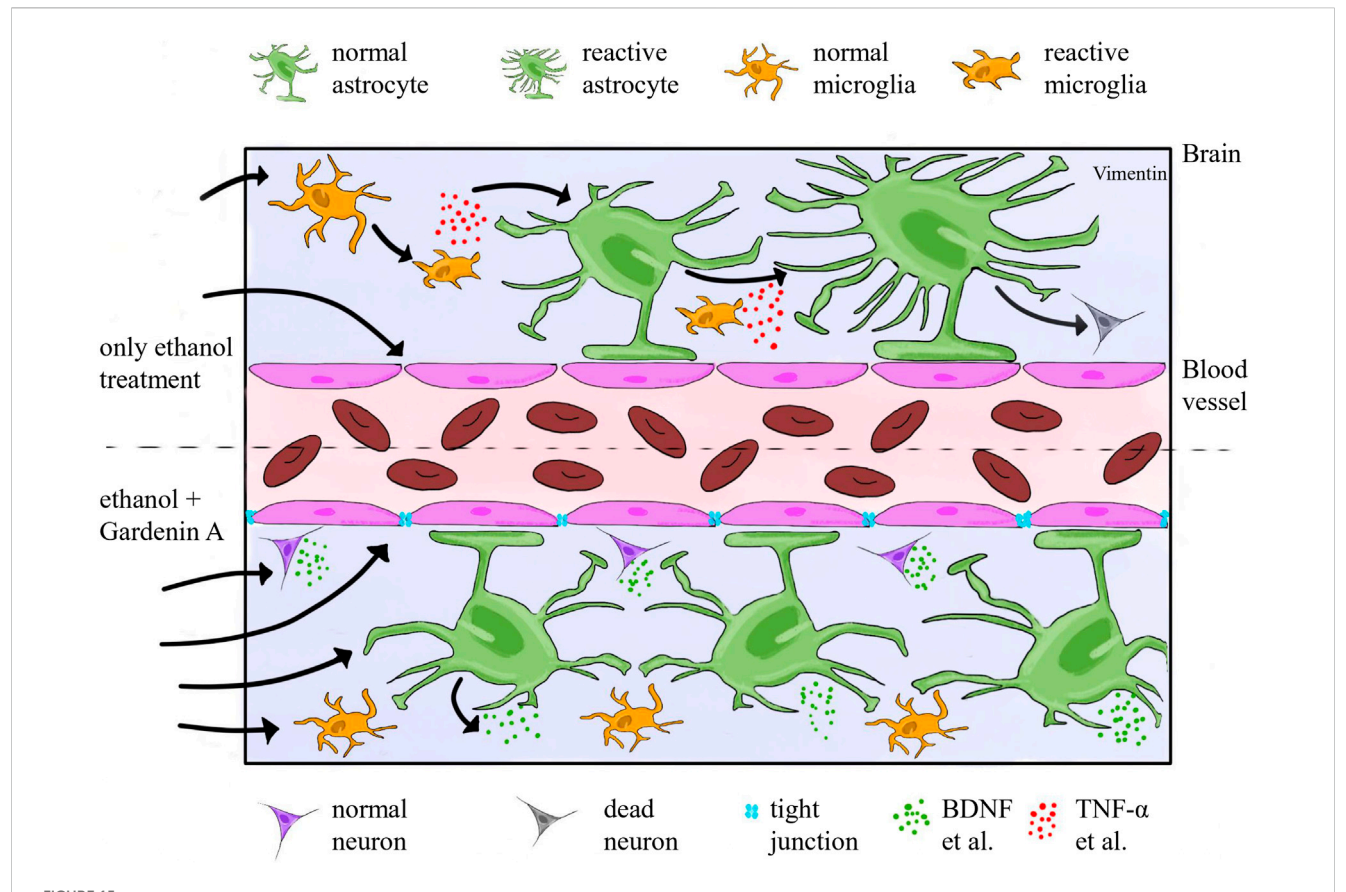


FIGURE 15
Schematic diagram showing cellular and molecular mechanisms occurring in the brain and BBB in the state of intoxication (upper half) and GarA provided as a drug along with ethanol (lower half), separated by dashed line. Ethanol exposure is associated with glial activation, increased proinflammatory cytokines such as TNFα, IL-6 and potential disruption of BBB. GarA is shown to be linked with modulation of neuronal and glial responses, including factors such as BDNF, Nrf2, HO-1 and IL-10. Image drawn using SketchBook app v6.0.4.

expression. Immunohistochemical and transcriptional data showed upregulation of vimentin and TNF $\alpha$  in ethanolexposed rats. GarA significantly reduced their levels, consistent with a potential role in modulating TLR4–NF- $\kappa$ B signaling, as previously implicated in ethanol-mediated neuroinflammation (Fernandez-Lizarbe et al., 2009). A previous study showed alcohol induced neurodegeneration due to binge ethanol consumption in rat model, where vimentin was upregulated due to ethanol-induced cell death (Kelso et al., 2011). Concurrently, the anti-inflammatory cytokine IL-10 was elevated, while PCSK9, a novel neuroinflammatory mediator in the liver–brain axis was downregulated by GarA (Lee et al., 2021). Furthermore, GarA also helped in reducing the protein expression of IL-6 and MCP-1.

Importantly, GarA treatment was associated with restored BDNF expression in both *in vitro* and *in vivo* models, suggesting potential support for synaptic plasticity, learning, and memory. While the upregulation of BDNF is promising, the direct causal linkage between GarA associated-BDNF restoration and neuroprotection remains to be confirmed. Ethanol-induced reductions in BDNF expression are well-documented and contribute to cognitive decline and neurodegeneration (Shafiee et al., 2023). The probable ability of GarA in upregulating BDNF,

surpassing control levels, might support its role in neuronal survival and regeneration.

Given the multi-target nature of ethanol-induced neurotoxicity, a network pharmacology analysis was undertaken to predict potential interacting pathways and validate the mechanistic scope of GarA. The integrated molecular docking and MD simulation results support the hypothesis that GarA exhibits a strong multitarget interaction profile relevant to ethanol-induced neurotoxicity. Docking and MD simulation results suggest that GarA may interact with BDNF, IL-6, and MCP-1, indicating potential associations with neurotrophic and inflammatory signaling pathways consistent with experimental observations. These proteins play pivotal roles in alcohol-related brain damage, BDNF is essential for neuronal survival and plasticity, while IL-6 and MCP-1 are central to glial activation and sustained neuroinflammation. Previously, molecular docking with TNF $\alpha$  and GarA has shown high binding affinity with a stable complex formation (Chadha et al., 2025).

The docking affinity of GarA across all three targets, combined with the observed conformational stability during MD simulations, indicates its probable potential to maintain prolonged interaction under physiological conditions. The low ligand RMSD values and stable protein backbones in the simulations further suggest that GarA can occupy and persist within the active sites without

significant disruption, enhancing its likelihood of effective biological modulation. MD simulations were performed as single 100-ns trajectories due to computational constraints; while replicates would provide error estimates, the detailed parameters, RMSD/RMSF profiles, and deposited files ensure reproducibility and offer meaningful insights into complex stability. Further, *in vitro* protein assays may help clarify the binding modes of GarA with these targets.

These findings align well with the results of network pharmacology, which highlighted TNF $\alpha$ , IL-6, and related pathways as key modulatory hubs in ethanol-induced damage. By simultaneously targeting proteins involved in inflammatory signaling and neuroprotection, GarA may offer a synergistic mode of action, suppress pro-inflammatory cascades while preserving or enhancing neurotrophic support (Figure 15). These associative findings support further investigation into GarA as a potential therapeutic candidate in alcohol-related neurodegenerative conditions.

The current study combined in vitro, in vivo, and in silico approaches to generate converging evidence that GarA is associated with modulation of neuroinflammatory neuroprotective pathways, including TNFa, BDNF, and Nrf2/ HO-1. Although direct perturbation studies with pathway-specific inhibitors or genetic knockdowns were not included, the consistency of findings across experimental systems provides strong support for the involvement of these signaling mechanisms. Future investigations incorporating such targeted interventions would help to further delineate mechanistic specificity. Further, given that sex-specific differences in neuroinflammation neurodegeneration are increasingly recognized, inclusion of both sexes in future studies will be essential to establish the broader relevance of these findings. From a translational perspective, the doses of GarA used in rodents (50 and 100 mg/kg) were guided by prior safety and efficacy reports; however, these doses cannot be directly extrapolated to humans due to interspecies differences in metabolism, pharmacokinetics, and bioavailability. Collection of pharmacokinetic and pharmacodynamic data, together with dosescaling studies, are required to evaluate clinical feasibility. Additionally, complementary models and longer-term experimental paradigms may be necessary to further validate and extend the translational relevance of these findings.

### Data availability statement

The original contributions presented in the study are included in the article/Supplementary Material, further inquiries can be directed to the corresponding author.

### **Ethics statement**

Ethical approval was not required for the studies on humans in accordance with the local legislation and institutional requirements because only commercially available established cell lines were used. The animal study was approved by Institutional Animal Ethics Committee of Charotar University of Science and Technology (Approval No. RPCP/IAEC/2023-24/R16). The study was

conducted in accordance with the local legislation and institutional requirements.

### **Author contributions**

PC: Conceptualization, Data curation, Formal Analysis, Methodology, Investigation, Validation, Visualization, Writing - original draft, Writing - review and editing. HA: Data curation, Investigation, Methodology, Visualization, Writing - original draft, Writing - review and editing. HS: Data curation. Investigation, Methodology, Visualization, Writing - original draft, Writing - review and editing. MP: Data curation, Investigation, Methodology, Visualization, Writing - original draft, Writing - review and editing. DS: Data curation, Investigation, Methodology, Visualization, Writing - original draft, Writing - review and editing. VT: Resources, Writing - original draft, Writing - review and editing. PM: Project administration, Resources, Supervision, Writing - original draft, Writing - review and editing.

### **Funding**

The author(s) declare that financial support was received for the research and/or publication of this article. For this research work, the contingency for procuring materials was provided by Lady Tata memorial Trusts, Bombay (India). They had also provided JRF and SRF fellowship to the main author (PC).

### Acknowledgements

The authors would like to thank PD Patel Institute of Applied Sciences (PDPIAS) and Ramanbhai Patel College of Pharmacy (RPCP), Charotar University of Science and Technology (CHARUSAT), for providing infrastructural facilities for smooth conduct of the current research work. A special note of thanks to Lady Tata Memorial Trusts (LTMT) for providing SRF to PC.

### Conflict of interest

The authors declare that the research was conducted in the absence of any commercial or financial relationships that could be construed as a potential conflict of interest.

The author(s) declared that they were an editorial board member of Frontiers, at the time of submission. This had no impact on the peer review process and the final decision.

### Generative AI statement

The author(s) declare that no Generative AI was used in the creation of this manuscript.

Any alternative text (alt text) provided alongside figures in this article has been generated by Frontiers with the support of artificial intelligence and reasonable efforts have been made to ensure

accuracy, including review by the authors wherever possible. If you identify any issues, please contact us.

### Publisher's note

All claims expressed in this article are solely those of the authors and do not necessarily represent those of their affiliated organizations, or those of the publisher, the editors and the reviewers. Any product that may be evaluated in this article, or claim that may be made by its manufacturer, is not guaranteed or endorsed by the publisher.

### References

Agabio, R., Lopez-Pelayo, H., Bruguera, P., Huang, S.-Y., Sardo, S., Pecina, M., et al. (2024). Efficacy of medications for the treatment of alcohol use disorder (AUD): a systematic review and meta-analysis considering baseline AUD severity. *Pharmacol. Res.* 209, 107454. doi:10.1016/j.phrs.2024.107454

Aghara, H., Chadha, P., and Mandal, P. (2024). Mitigative effect of graphene oxide nanoparticles in maintaining gut-liver homeostasis against alcohol injury. Gastroenterol. Insights 15, 574–587. doi:10.3390/gastroent15030042

Alonso-Castro, A. J., Gasca-Martínez, D., Cortez-Mendoza, L. V., Alba-Betancourt, C., Ruiz-Padilla, A. J., and Zapata-Morales, J. R. (2020). Evaluation of the neuropharmacological effects of gardenin A in mice. *Drug Dev. Res.* 81, 600–608. doi:10.1002/ddr.21659

Anand, S. K., Ahmad, M. H., Sahu, M. R., Subba, R., and Mondal, A. C. (2023). Detrimental effects of alcohol-induced inflammation on brain health: from neurogenesis to neurodegeneration. *Cell Mol. Neurobiol.* 43, 1885–1904. doi:10.1007/s10571-022-01308-2

Bandegi, A. R., Rashidy-Pour, A., Vafaei, A. A., and Ghadrdoost, B. (2014). Protective effects of Crocus sativus L. extract and crocin against chronic-stress induced oxidative damage of brain, liver and kidneys in rats. *Adv. Pharm. Bull.* 4, 493–499. doi:10.5681/apb.2014.073

Bankfalvi, A., Navabi, H., Bier, B., Bocker, W., Jasani, B., and Schmid, K. W. (1994). Wet autoclave pretreatment for antigen retrieval in diagnostic immunohistochemistry. *J. Pathol.* 174, 223–228. doi:10.1002/path.1711740312

Beisswenger, T. B., Holmquist, B., and Vallee, B. L. (1985). chi-ADH is the sole alcohol dehydrogenase isozyme of Mammalian brains: implications and inferences. *Proc. Natl. Acad. Sci.* 82, 8369–8373. doi:10.1073/pnas.82.24.8369

Bowers, K. J., Chow, D. E., Xu, H., Dror, R. O., Eastwood, M. P., Gregersen, B. A., et al. (2006). "Scalable algorithms for molecular dynamics simulations on commodity clusters," in *ACM/IEEE SC 2006 conference (SC'06)* (IEEE), 43. doi:10.1109/SC.2006.54

Bustos-Rangel, A., Muñoz-Cabrera, J., Cuca, L., Arboleda, G., Ávila Murillo, M., and Sandoval-Hernández, A. G. (2023). Neuroprotective and antioxidant activities of Colombian plants against paraquat and C2-ceramide exposure in SH-SY5Y cells. *Front. Nat. Prod.* 2, 1169182. doi:10.3389/fntpr.2023.1169182

Carito, V., Ceccanti, M., Cestari, V., Natella, F., Bello, C., Coccurello, R., et al. (2017). Olive polyphenol effects in a mouse model of chronic ethanol addiction. *Nutrition* 33, 65–69. doi:10.1016/j.nut.2016.08.014

Carmichael, F. J., Israel, Y., Crawford, M., Minhas, K., Saldivia, V., Sandrin, S., et al. (1991). Central nervous system effects of acetate: contribution to the central effects of ethanol. *J. Pharmacol. Exp. Ther.* 259, 403–408. doi:10.1016/S0022-3565(25)20542-0

Carrino, D., Branca, J. J. V., Becatti, M., Paternostro, F., Morucci, G., Gulisano, M., et al. (2021). Alcohol-induced blood-brain barrier impairment: an *in vitro* study. *Int. J. Environ. Res. Public Health* 18, 2683–14. doi:10.3390/ijerph18052683

Chadha, P., Aghara, H., Johnson, D., Sharma, D., Odedara, M., Patel, M., et al. (2025). Gardenin A alleviates alcohol-induced oxidative stress and inflammation in HepG2 and Caco2 cells *via* AMPK/Nrf2 pathway. *Bioorg Chem.* 161, 108543. doi:10.1016/j.bioorg. 2025.108543

Chiu, S. P., Wu, M. J., Chen, P. Y., Ho, Y. R., Tai, M. H., Ho, C. T., et al. (2013). Neurotrophic action of 5-hydroxylated polymethoxyflavones: 5-Demethylnobiletin and gardenin A stimulate neuritogenesis in PC12 cells. *J. Agric. Food Chem.* 61, 9453–9463. doi:10.1021/jf4024678

Crews, F. T. (2008). AlcoholRelated neurodegeneration and recovery mechanisms from animal models. *Alcohol Res. Health.* 31, 377–388.

Daina, A., Michielin, O., and Zoete, V. (2019). SwissTargetPrediction: updated data and new features for efficient prediction of protein targets of small molecules. *Nucleic Acids Res.* 47, W357–W364. doi:10.1093/nar/gkz382

### Supplementary material

The Supplementary Material for this article can be found online at: https://www.frontiersin.org/articles/10.3389/fphar.2025.1681403/full#supplementary-material

SUPPLEMENTARY VIDEO 1

Simulation video file BDNF-GarA

SUPPLEMENTARY VIDEO 2

Simulation video file IL6-GarA

SUPPLEMENTARY VIDEO 3

Simulation video file MCP1-GarA.

Das, S. K., Hiran, K. R., Mukherjee, S., and Vasudevan, D. M. (2007). Oxidative stress is the primary event: effects of ethanol consumption in brain. *Indian J. Clin. Biochem.* 22, 99–104. doi:10.1007/BF02912890

Fadda, F., and Rossetti, Z. L. (1998). Chronic ethanol consumption:from neuroadaptation to neurodegeneration. *Prog. Neurobiol.* 56, 385–431. doi:10.1016/S0301-0082(98)00032-X

Feng, Y., Ju, Y., Yan, Z., Ji, M., Yang, M., Wu, Q., et al. (2022). Protective role of wogonin following traumatic brain injury by reducing oxidative stress and apoptosis *via* the PI3K/Nrf2/HO-1 pathway. *Int. J. Mol. Med.* 49, 53. doi:10.3892/ijmm.2022.5109

Fernandez-Lizarbe, S., Pascual, M., and Guerri, C. (2009). Critical role of TLR4 response in the activation of Microglia induced by ethanol. *J. Immunol.* 183, 4733–4744. doi:10.4049/jimmunol.0803590

Fikry, H., Saleh, L. A., and Abdel Gawad, S. (2022). Neuroprotective effects of curcumin on the cerebellum in a rotenone-induced Parkinson's Disease Model. *CNS Neurosci. Ther.* 28, 732–748. doi:10.1111/cns.13805

Filimonov, D. A., Lagunin, A. A., Gloriozova, T. A., Rudik, A. V., Druzhilovskii, D. S., Pogodin, P. V., et al. (2014). Prediction of the biological activity spectra of organic compounds using the Pass online web resource. *Chem. Heterocycl. Compd. (N Y)* 50, 444–457. doi:10.1007/s10593-014-1496-1

Friesner, R. A., Murphy, R. B., Repasky, M. P., Frye, L. L., Greenwood, J. R., Halgren, T. A., et al. (2006). Extra precision glide: docking and scoring incorporating a model of hydrophobic enclosure for protein–ligand complexes. *J. Med. Chem.* 49, 6177–6196. doi:10.1021/jm0512560

Galter, D., Carmine, A., Buervenich, S., Duester, G., and Olson, L. (2003). Distribution of class I, III and IV alcohol dehydrogenase mRNAs in the adult rat, mouse and human brain. *Eur. J. Biochem.* 270, 1316–1326. doi:10.1046/j.1432-1033.2003.03502.x

Ge, S. X., Jung, D., and Yao, R. (2020). ShinyGO: a graphical gene-set enrichment tool for animals and plants. *Bioinformatics* 36, 2628–2629. doi:10.1093/bioinformatics/btz931

Ghosh, B., Yadav, S., and Sharma, R. K. (2021). Aluminium induced neurodegeneration in Rat cerebrum in presence of ethanol Co-exposure. *J. Clin. DIAGNOSTIC Res.* doi:10.7860/jcdr/2021/47733.15022

Guerri, C., and Pascual, M. (2019). Role of neuroinflammation in ethanol neurotoxicity. *Adv. Neurotoxicol.*, 259–294. doi:10.1016/bs.ant.2018.10.009

Hack, W., Gladen-Kolarsky, N., Chatterjee, S., Liang, Q., Maitra, U., Ciesla, L., et al. (2024). Gardenin A treatment attenuates inflammatory markers, synuclein pathology and deficits in tyrosine hydroxylase expression and improves cognitive and motor function in A53T-α-syn mice. *Biomed. Pharmacother.* 173, 116370. doi:10.1016/j. biopha.2024.116370

Haorah, J., Knipe, B., Leibhart, J., Ghorpade, A., and Persidsky, Y. (2005). Alcoholinduced oxidative stress in brain endothelial cells causes blood-brain barrier dysfunction. *J. Leukoc. Biol.* 78, 1223–1232. doi:10.1189/jlb.0605340

Haorah, J., Knipe, B., Gorantla, S., Zheng, J., and Persidsky, Y. (2007a). Alcoholinduced blood-brain barrier dysfunction is mediated *via* inositol 1,4,5-triphosphate receptor (IP 3 r)-gated intracellular calcium release. *J. Neurochem.* 100, 324–336. doi:10. 1111/j.1471-4159.2006.04245.x

Haorah, J., Ramirez, S. H., Schall, K., Smith, D., Pandya, R., and Persidsky, Y. (2007b). Oxidative stress activates protein tyrosine kinase and matrix metalloproteinases leading to blood–brain barrier dysfunction. *J. Neurochem.* 101, 566–576. doi:10.1111/j.1471-4159.2006.04393.x

Holloway, K. N., Douglas, J. C., Rafferty, T. M., Kane, C. J. M., and Drew, P. D. (2023). Ethanol induces neuroinflammation in a chronic plus binge mouse model of alcohol use disorder *via* TLR4 and MyD88-Dependent signaling. *Cells* 12, 2109. doi:10.3390/cells12162109

- Ieraci, A., and Herrera, D. G. (2006). Nicotinamide protects against ethanol-induced apoptotic neurodegeneration in the developing mouse brain. *PLoS Med.* 3, e101–e557. doi:10.1371/journal.pmed.0030101
- Jin, S., Cao, Q., Yang, F., Zhu, H., Xu, S., Chen, Q., et al. (2021). Brain ethanol metabolism by astrocytic ALDH2 drives the behavioural effects of ethanol intoxication. *Nat. Metab.* 3, 337–351. doi:10.1038/s42255-021-00357-z
- Jorgensen, W. L., Chandrasekhar, J., Madura, J. D., Impey, R. W., and Klein, M. L. (1983). Comparison of simple potential functions for simulating liquid water. *J. Chem. Phys.* 79, 926–935. doi:10.1063/1.445869
- Kamal, H., Tan, G. C., Ibrahim, S. F., Shaikh, M. F., Mohamed, I. N., Mohamed, R. M. P., et al. (2020). Alcohol use disorder, neurodegeneration, alzheimer's and Parkinson's disease: interplay between oxidative stress, neuroimmune response and excitotoxicity. *Front. Cell Neurosci.* 14, 282. doi:10.3389/fncel.2020.00282
- Kang, S., Piao, Y., Kang, Y. C., Lim, S., and Pak, Y. K. (2020). Qi-activating quercetin alleviates mitochondrial dysfunction and neuroinflammation *in vivo* and *in vitro*. *Arch. Pharm. Res.* 43, 553–566. doi:10.1007/s12272-020-01238-x
- Keiser, M. J., Roth, B. L., Armbruster, B. N., Ernsberger, P., Irwin, J. J., and Shoichet, B. K. (2007). Relating protein pharmacology by ligand chemistry. *Nat. Biotechnol.* 25, 197–206. doi:10.1038/nbt1284
- Kelso, M. L., Liput, D. J., Eaves, D. W., and Nixon, K. (2011). Upregulated vimentin suggests new areas of neurodegeneration in a model of an alcohol use disorder. *Neuroscience* 197, 381–393. doi:10.1016/j.neuroscience.2011.09.019
- Kinoshita, T., and Firman, K. (1996). Highly oxygenated flavonoids from Murraya paniculata. *Phytochemistry* 42, 1207–1210. doi:10.1016/0031-9422(96)00058-1
- Lee, H. J., Noh, Y. H., Lee, D. Y., Kim, Y. S., Kim, K. Y., Chung, Y. H., et al. (2005). Baicalein attenuates 6-hydroxydopamine-induced neurotoxicity in SH-SY5Y cells. *Eur. J. Cell Biol.* 84, 897–905. doi:10.1016/j.ejcb.2005.07.003
- Lee, J. S., O'connell, E. M., Pacher, P., and Lohoff, F. W. (2021). Pcsk9 and the gutliver-brain axis: a novel therapeutic target for immune regulation in alcohol use disorder. *J. Clin. Med.* 10, 1758. doi:10.3390/jcm10081758
- Li, X., He, G., Mu, X., Xu, B., Tian, S., Yu, X., et al. (2012). Protective effects of baicalein against rotenone-induced neurotoxicity in PC12 cells and isolated rat brain mitochondria. *Eur. J. Pharmacol.* 674, 227–233. doi:10.1016/j.ejphar.2011.09.181
- Li, C., Li, J., Xu, G., and Sun, H. (2020). Influence of chronic ethanol consumption on apoptosis and autophagy following transient focal cerebral ischemia in Male mice. *Sci. Rep.* 10, 6164. doi:10.1038/s41598-020-63213-2
- Litov, L., Petkov, P., Rangelov, M., Ilieva, N., Lilkova, E., Todorova, N., et al. (2021). Molecular mechanism of the anti-inflammatory action of heparin. *Int. J. Mol. Sci.* 22, 10730. doi:10.3390/ijms221910730
- Liu, X., Ouyang, S., Yu, B., Liu, Y., Huang, K., Gong, J., et al. (2010). PharmMapper server: a web server for potential drug target identification using pharmacophore mapping approach. *Nucleic Acids Res.* 38, W609–W614. doi:10.1093/nar/gkq300
- Liu, H., Meng, W., Zhao, D., Ma, Z., Zhang, W., Chen, Z., et al. (2023). Study on mechanism of action of total flavonoids from Cortex Juglandis Mandshuricae against alcoholic liver disease based on "gut-liver axis.". *Front. Pharmacol.* 13, 1074286. doi:10. 3389/fphar.2022.1074286
- Lu, C., Wu, C., Ghoreishi, D., Chen, W., Wang, L., Damm, W., et al. (2021). OPLS4: improving force field accuracy on challenging regimes of chemical space. *J. Chem. Theory Comput.* 17, 4291–4300. doi:10.1021/acs.jctc.1c00302
- Lubkowski, J., Bujacz, G., Boqué, L., Peter, J. D., Tracy, M. H., and Alexander, W. (1997). The structure of MCP-1 in two crystal forms provides a rare example of variable Quaternary interactions. *Nat. Struct. Mol. Biol.* 4, 64–69. doi:10.1038/nsb0197-64
- MacKillop, J., Agabio, R., Feldstein Ewing, S. W., Heilig, M., Kelly, J. F., Leggio, L., et al. (2022). Hazardous drinking and alcohol use disorders. *Nat. Rev. Dis. Prim.* 8, 80. doi:10.1038/s41572-022-00406-1
- Madhavi Sastry, G., Adzhigirey, M., Day, T., Annabhimoju, R., and Sherman, W. (2013). Protein and ligand preparation: parameters, protocols, and influence on virtual screening enrichments. *J. Comput. Aided Mol. Des.* 27, 221–234. doi:10.1007/s10822-013-9644-8
- Maitra, U., Harding, T., Liang, Q., and Ciesla, L. (2021). GardeninA confers neuroprotection against environmental toxin in a drosophila model of Parkinson's disease. *Commun. Biol.* 4, 162. doi:10.1038/s42003-021-01685-2
- Martín-González, C., González-Arnay, E., Fernández-Rodríguez, C. M., García-Rodríguez, A., and González-Reimers, E. (2022). "Alcohol and brain-derived neurotrophic factor (BDNF)," in *Handbook of substance misuse and addictions* (Springer International Publishing), 1–27. doi:10.1007/978-3-030-67928-6\_182-1
- Martínez, S. E., Vaglenova, J., Sabrià, J., Martínez, M. C., Farrés, J., and Parés, X. (2001). Distribution of alcohol dehydrogenase mRNA in the rat central nervous system. *Eur. J. Biochem.* 268, 5045–5056. doi:10.1046/j.0014-2956.2001.02416.x-i2
- Martyna, G. J., Tobias, D. J., and Klein, M. L. (1994). Constant pressure molecular dynamics algorithms. J. Chem. Phys. 101, 4177–4189. doi:10.1063/1.467468
- Mews, P., Egervari, G., Nativio, R., Sidoli, S., Donahue, G., Lombroso, S. I., et al. (2019). Alcohol metabolism contributes to brain histone acetylation. *Nature* 574, 717–721. doi:10.1038/s41586-019-1700-7

- Miguel-Hidalgo, J. J. (2018). Molecular neuropathology of astrocytes and oligodendrocytes in alcohol use disorders. *Front. Mol. Neurosci.* 11, 78. doi:10.3389/fnmol.2018.00078
- Motaghinejad, M., Mashayekh, R., Motevalian, M., and Safari, S. (2021). The possible role of CREB-BDNF signaling pathway in neuroprotective effects of minocycline against alcohol-induced neurodegeneration: molecular and behavioral evidences. *Fundam. Clin. Pharmacol.* 35, 113–130. doi:10.1111/fcp.12584
- Nosé, S. (1984). A unified formulation of the constant temperature molecular dynamics methods. *J. Chem. Phys.* 81, 511–519. doi:10.1063/1.447334
- Oliveros, J. C. (2015). Venny. An interactive tool for comparing lists with Venn's diagrams. Available online at: https://bioinfogp.cnb.csic.es/tools/venny/index.html (Accessed July 21, 2025).
- Paccosi, S., Musilli, C., Mangano, G., Guglielmotti, A., and Parenti, A. (2012). The monocyte chemotactic protein synthesis inhibitor bindarit prevents mesangial cell proliferation and extracellular matrix remodeling. *Pharmacol. Res.* 66, 526–535. doi:10. 1016/j.phrs.2012.09.006
- Pascual, M., Baliño, P., Aragón, C. M. G., and Guerri, C. (2015). Cytokines and chemokines as biomarkers of ethanol-induced neuroinflammation and anxiety-related behavior: role of TLR4 and TLR2. *Neuropharmacology* 89, 352–359. doi:10.1016/j.neuropharm.2014.10.014
- Patel, F., and Mandal, P. (2018). "Effect of alcohol on brain development," in Drug Addiction, (InTech). doi:10.5772/intechopen.73693
- Patel, F., Parwani, K., Patel, D., and Mandal, P. (2021). Metformin and probiotics interplay in amelioration of ethanol-induced oxidative stress and inflammatory response in an *in vitro* and *in vivo* model of hepatic injury. *Mediat. Inflamm.* 2021, 6636152–31. doi:10.1155/2021/6636152
- Petrella, C., Carito, V., Carere, C., Ferraguti, G., Ciafrè, S., Natella, F., et al. (2020). Oxidative stress inhibition by resveratrol in alcohol-dependent mice. *Nutrition* 79-80, 110783–80. doi:10.1016/j.nut.2020.110783
- Piñero, J., Ramírez-Anguita, J. M., Saüch-Pitarch, J., Ronzano, F., Centeno, E., Sanz, F., et al. (2019). The DisGeNET knowledge platform for disease genomics: 2019 update. *Nucleic Acids Res.* doi:10.1093/nar/gkz1021
- Qiao, Y., Yuan, Q., and Liu, Z. (2024). Huangqi Gegen decoction ameliorates alcoholinduced cognitive dysfunction *via* attenuating oxidative stress and enhancing bloodbrain barrier integrity in rats through the Keap1-Nrf2/HO-1 signaling pathway. *Iran. J. Basic Med. Sci.* 27, 1331–1339. doi:10.22038/ijbms.2024.77415.16737
- Qin, L., and Crews, F. T. (2012). Chronic ethanol increases systemic TLR3 agonist-induced neuroinflammation and neurodegeneration. *J. Neuroinflammation* 9, 130. doi:10.1186/1742-2094-9-130
- Raivio, N., Tiraboschi, E., Saarikoski, S. T., Castrén, E., and Kiianmaa, K. (2012). Brain-derived neurotrophic factor expression after acute administration of ethanol. *Eur. J. Pharmacol.* 687, 9–13. doi:10.1016/j.ejphar.2012.04.021
- Rath, M., Figueroa, A. M., Zhang, P., Stevens, S. M., and Liu, B. (2022). Establishment of a simple and versatile evaporation compensation model for *in vitro* chronic ethanol treatment: impact on neuronal viability. *Neuroglia* 3, 61–72. doi:10.3390/neuroglia3020004
- Reid, C., Rushe, M., Jarpe, M., van Vlijmen, H., Dolinski, B., Qian, F., et al. (2006). Structure activity relationships of monocyte chemoattractant proteins in complex with a blocking antibody. *Protein Eng. Des. Sel.* 19, 317–324. doi:10.1093/protein/gzl015
- Robinson, R. C., Radziejewski, C., Stuart, D. I., and Jones, E. Y. (1995). Structure of the brain-derived Neurotrophic Factor/Neurotrophin 3 heterodimer. *Biochemistry* 34, 4139–4146. doi:10.1021/bi00013a001
- Ruiz-Uribe, N. E., and Bracko, O. (2020). Brain and blood extraction for immunostaining, protein, and RNA measurements after long-term two photon imaging in mice. doi:10.21203/rs.3.pex-838/v1
- Sangeet, S., Khan, A., Mahanta, S., Roy, N., Das, S. K., Mohanta, Y. K., et al. (2023). Computational analysis of *Bacopa monnieri* (L.) wettst. Compounds for drug development against neurodegenerative disorders. *Curr. Comput. Aided Drug Des.* 19, 24–36. doi:10.2174/1573409918666221010103652
- Shafiee, A., Jafarabady, K., Rafiei, M. A., Beiky, M., Seighali, N., Golpayegani, G., et al. (2023). Effect of alcohol on brain-derived neurotrophic factor (BDNF) blood levels: a systematic review and meta-analysis. *Sci. Rep.* 13, 17554. doi:10.1038/s41598-023-44798-w
- Shannon, P., Markiel, A., Ozier, O., Baliga, N. S., Wang, J. T., Ramage, D., et al. (2003). Cytoscape: a software environment for integrated models of biomolecular interaction networks. *Genome Res.* 13, 2498–2504. doi:10.1101/gr.1239303
- Somers, W., Stahl, M., and Seehra, J. S. (1997). 1.9 acrystal structure of interleukin 6: implications for a novel mode of receptor dimerization and signaling. *EMBO J.* 16, 989–997. doi:10.1093/emboj/16.5.989
- Stelzer, G., Rosen, N., Plaschkes, I., Zimmerman, S., Twik, M., Fishilevich, S., et al. (2016). The GeneCards suite: from gene data mining to disease genome sequence analyses. *Curr. Protoc. Bioinforma.* 54 (1), 1.30.1–1.30.33. doi:10.1002/cpbi.5
- Suvarna, S. K., Layton, C., and Bancroft, J. D. (2012). Bancroft's theory and practice of histological techniques. 7th Edn. London: Churchill Livingstone.

Szklarczyk, D., Kirsch, R., Koutrouli, M., Nastou, K., Mehryary, F., Hachilif, R., et al. (2023). The STRING database in 2023: protein–protein association networks and functional enrichment analyses for any sequenced genome of interest. *Nucleic Acids Res.* 51, D638–D646. doi:10.1093/nar/gkac1000

Tapia-Arancibia, L., Rage, F., Givalois, L., Dingeon, P., Arancibia, S., and Beaugé, F. (2001). Effects of alcohol on brain-derived neurotrophic factor mRNA expression in discrete regions of the Rat Hippocampus and Hypothalamus. *J. Neurosci. Res.* 63, 200–208. doi:10.1002/1097-4547(20010115)63:2<200::AID-JNR1012>3.0.CO;2-Q

Tiwari, V., Kuhad, A., and Chopra, K. (2010). Epigallocatechin-3-gallate ameliorates alcohol-induced cognitive dysfunctions and apoptotic neurodegeneration in the developing rat brain. *Int. J. Neuropsychopharmacol.* 13, 1053–1066. doi:10.1017/S146114571000060X

Tjiptaningrum, A., Kurniati, I., Fadilah, F., Susantiningsih, T., Prawiningrum, A. F., Utari, W. D., et al. (2024). Protein interaction analysis and molecular simulation of the anti-inflammatory activities in Melaleuca cajuputi extract against COVID-19. *Int. J. Inflam.* 2024, 5568294. doi:10.1155/ijin/5568294

Togre, N. S., Mekala, N., Bhoj, P. S., Mogadala, N., Winfield, M., Trivedi, J., et al. (2024). Neuroinflammatory responses and blood-brain barrier injury in chronic alcohol exposure: role of purinergic P2  $\times$  7 receptor signaling. *J. Neuroinflammation* 21, 244. doi:10.1186/s12974-024-03230-4

Toppo, E., Darvin, S. S., Esakkimuthu, S., Stalin, A., Balakrishna, K., Sivasankaran, K., et al. (2017). Antihyperlipidemic and hepatoprotective effects of Gardenin A in cellular and high fat diet fed rodent models. *Chem. Biol. Interact.* 269, 9–17. doi:10.1016/j.cbi.2017.03.013

Varadinova, M. G., Valcheva-Traykova, M. L., and Boyadjieva, N. I. (2019). "Alcoholinduced oxidative stress in the brain: suggested mechanisms, associated disorders, and therapeutic strategies," in *Neuroscience of alcohol: mechanisms and treatment* (Elsevier), 505–513. doi:10.1016/B978-0-12-813125-1.00052-0

Vetrivel, U., Ravichandran, S. B., Kuppan, K., Mohanlal, J., Das, U. N., and Narayanasamy, A. (2012). Agonistic effect of polyunsaturated fatty acids (PUFAs) and its metabolites on brain-derived neurotrophic factor (BDNF) through molecular docking simulation. *Lipids Health Dis.* 11, 109. doi:10.1186/1476-511X-11-109

Volkow, N. D., Kim, S. W., Wang, G.-J., Alexoff, D., Logan, J., Muench, L., et al. (2013). Acute alcohol intoxication decreases glucose metabolism but increases acetate uptake in the human brain. *Neuroimage* 64, 277–283. doi:10.1016/j.neuroimage.2012.08.057

Vore, A. S., and Deak, T. (2022). "Alcohol, inflammation, and blood-brain barrier function in health and disease across development," in *International review of neurobiology* (Academic Press Inc.), 209–249. doi:10.1016/bs.irn.2021.06.009

Wang, Q., Haseeb, A., Meng, X., Feng, Y., Hussain, A., and Yang, P. (2022). Telocytes in the esophageal wall of chickens: a tale of subepithelial telocytes. *Poult. Sci.* 101, 101859. doi:10.1016/j.psj.2022.101859

Ward, R. J., Lallemand, F., and de Witte, P. (2009). Biochemical and neurotransmitter changes implicated in alcohol-induced brain damage in chronic or "binge drinking" alcohol abuse. *Alcohol Alcohol.* 44, 128–135. doi:10.1093/alcalc/agn100

Wei, J., Dai, Y., Wen, W., Li, J., Ye, L. L., Xu, S., et al. (2021). Blood-brain barrier integrity is the primary target of alcohol abuse. *Chem. Biol. Interact.* 337, 109400. doi:10. 1016/j.cbi.2021.109400

Wen, W., Li, H., and Luo, J. (2022). Potential role of MANF, an ER stress responsive neurotrophic factor, in protecting against alcohol neurotoxicity. *Mol. Neurobiol.* 59, 2992–3015. doi:10.1007/s12035-022-02786-7

Wilson, D. F., and Matschinsky, F. M. (2020). Ethanol metabolism: the good, the bad, and the ugly. *Med. Hypotheses* 140, 109638. doi:10.1016/j.mehy.2020.109638

World Health Organization (2024). Alcohol. Available online at: https://www.who.int/news-room/fact-sheets/detail/alcohol (Accessed July 15, 2025).

Yang, F., and Luo, J. (2015). Endoplasmic Reticulum stress and ethanol neurotoxicity. *Biomolecules* 5, 2538–2553. doi:10.3390/biom5042538

Yang, W. L., Chen, S. Y., Ho, C. Y., and Yen, G. C. (2020). "Citrus flavonoids suppress IL-5 and ROS through distinct pathways in PMA/ionomycin-induced EL-4 cells," in *Food and function* (London: Royal Society of Chemistry), 824–833. doi:10.1039/c9fo02815c

Yao, Z.-J., Dong, J., Che, Y.-J., Zhu, M.-F., Wen, M., Wang, N.-N., et al. (2016). TargetNet: a web service for predicting potential drug–target interaction profiling *via* multi-target SAR models. *J. Comput. Aided Mol. Des.* 30, 413–424. doi:10.1007/s10822-016-9915-2

Ye, J., Coulouris, G., Zaretskaya, I., Cutcutache, I., Rozen, S., and Madden, T. L. (2012). Primer-BLAST: a tool to design target-specific primers for polymerase chain reaction. *BMC Bioinforma*. 13, 134. doi:10.1186/1471-2105-13-134

Zhang, Z. J., Wang, Z., Zhang, X. Y., Ying, K., Liu, J. X., and Wang, Y. Y. (2005). Gene expression profile induced by oral administration of baicalin and gardenin after focal brain ischemia in rats. *Acta Pharmacol. Sin.* 26, 307–314. doi:10.1111/j.1745-7254.2005. 00051.x

Zhang, L., Wang, J., Yan, Y., Xiang, L., Zhai, X., Cai, L., et al. (2025). Vimentin fragmentation and its role in amyloid-beta plaque deposition in alzheimer's disease. *Int. J. Mol. Sci.* 26, 2857. doi:10.3390/ijms26072857

Zimatkin, S. M., Pronko, S. P., Vasiliou, V., Gonzalez, F. J., and Deitrich, R. A. (2006). Enzymatic mechanisms of ethanol oxidation in the brain. *Alcohol Clin. Exp. Res.* 30, 1500–1505. doi:10.1111/j.1530-0277.2006.00181.x

Zou, J., and Crews, F. T. (2012). Inflammasome-IL-1 $\beta$  signaling mediates ethanol inhibition of hippocampal neurogenesis. *Front. Neurosci.* 6, 77. doi:10.3389/fnins. 2012.00077